Title: Observational signatures of transuranic fission fragments in stars

Authors: Ian U. Roederer[1,2]*, Nicole Vassh[3], Erika M. Holmbeck[4,5,2], Matthew R. Mumpower[6,7,2], Rebecca Surman[8,2], John J. Cowan[9], Timothy C. Beers[8,2], Rana Ezzeddine[10,2], Anna Frebel[11,2], Terese T. Hansen[12], Vinicius M. Placco[13], Charli M. Sakari[14]

Affiliations:

[1]Department of Astronomy, University of Michigan; Ann Arbor, MI, USA.

[2]Joint Institute for Nuclear Astrophysics - Chemical Evolution of the Elements (JINA-CEE); USA.

[3]TRIUMF; Vancouver, BC, Canada.

[4]Carnegie Observatories; Pasadena, CA, USA.

[5]Hubble Fellow.

[6]Theoretical Division, Los Alamos National Laboratory; Los Alamos, NM, USA.

[7]Center for Theoretical Astrophysics, Los Alamos National Laboratory; Los Alamos, NM, USA.

[8]Department of Physics and Astronomy, University of Notre Dame; Notre Dame, IN, USA.

[9]Homer L. Dodge Department of Physics and Astronomy, University of Oklahoma; Norman, OK, USA.

[10]Department of Astronomy, University of Florida, Bryant Space Science Center; Gainesville, FL, USA.

[11]Department of Physics and Kavli Institute for Astrophysics and Space Research, Massachusetts Institute of Technology; Cambridge, MA, USA.

[12]Department of Astronomy, Stockholm University, AlbaNova University Center, SE-106 91 Stockholm, Sweden.

[13]NSF's NOIRLab; Tucson, AZ, USA.

[14]Department of Physics and Astronomy, San Francisco State University; San Francisco, CA, USA.

*Corresponding author. Email: iur@umich.edu

Abstract:

The heaviest elements observed in the universe are produced by the rapid neutron-capture process (r-process). Its termination among transuranic nuclei is poorly understood because these elements are inaccessible to experiments, forcing nuclear models to extrapolate from limited constraints. We show that the elements Ru, Rh, Pd, and Ag (atomic numbers $44 \leq Z \leq 47$, mass numbers $99 \leq A \leq 110$) exhibit a correlation with abundances of heavier elements ($63 \leq Z \leq 78$, $A > 150$) that is not shared by their immediate neighbors ($34 \leq Z \leq 42$ and $48 \leq Z \leq 62$) for stars that are enhanced in r-process elements. Coproduction via fission fragments of transuranic nuclei provides the most compelling explanation for this behavior. We conclude that this signature provides the first evidence that neutron-rich fissioning nuclei with mass numbers >260 are produced in r-process events, such as neutron-star mergers.

One-Sentence Summary:

A meta-analysis of stellar chemical abundances uncovers trends indicative of fission of the heaviest elements.

Understanding the origin of the elements is one of the major challenges of modern astrophysics. Stars and stellar remnants synthesize the heaviest elements listed on the periodic table through the rapid neutron-capture process, or r-process. The 2017 merger of a pair of neutron stars detected in gravitational waves and electromagnetic radiation *(1)* established these types of events as sites where the r-process occurs. The composition of material ejected constrains the conditions present during the merger *(2)* and properties of the progenitor neutron stars, including their equation of state *(3)*. Freshly produced lanthanide elements ($57 \leq Z \leq 71$) *(4, 5)* and Sr ($Z = 38$) *(6)* were likely present in the ejecta of that 2017 event, but otherwise its detailed chemical composition could not be inferred from either the light curve or spectra of its afterglow.

In contrast, the detailed compositions of a small number of ancient stars in the Milky Way can be derived from hundreds of absorption features of more than 40 r-process elements detectable in their spectra. The abundance patterns of heavy r-process elements found in these stars are similar, which is often referred to as the "universality" of the r-process. The chemical inventory of each star links directly to the ejecta of an individual r-process event, such as a neutron star merger or a rare type of supernova that occurred in the early Universe and enriched the gas from which these stars formed *(7)*.

We assemble a sample of 42 stars in the Milky Way from data presented in 35 studies in the literature *(8)*. We select stars whose heavy elements were formed via the r-process, without contamination from other processes, such as the slow neutron-capture process (s-process). We follow common practice in adopting the [Fe/H] ratio (defined as $\log_{10}(N_{\mathrm{Fe}}) - \log_{10}(N_{\mathrm{Fe}})_{\odot}$, where N is the number density and the $\odot$ subscript indicates the Solar value) as a measure of the overall metal enrichment of a star, and the [Eu/Fe] ratio (defined as $\log_{10}(N_{\mathrm{Eu}}/N_{\mathrm{Fe}}) - \log_{10}(N_{\mathrm{Eu}}/N_{\mathrm{Fe}})_{\odot}$) as a measure of the enhancement of r-process elements relative to the overall metal enrichment. Our sample spans $-3.57 \leq$ [Fe/H] ≤ -0.99 and $-0.52 \leq$ [Eu/Fe] $\leq +1.69$ (Tab. S1–S4). Fig. 1 illustrates the heavy-element abundance patterns in these stars (see also Fig. S1 and S2). Stars with higher [Eu/Fe] ratios, which are marked with larger symbols, generally exhibit abundances of some elements (including Ru, Rh, Pd, Ag, Gd, Tb, Dy, and Yb) that are slightly enhanced relative to stars with lower [Eu/Fe] ratios. This excess is not expected in the paradigm of r-process universality, and we now aim to explain it.

We empirically calculate a baseline abundance pattern (Tab. S5 and S6) using the 13 stars (30% of the sample) with the lowest levels of r-process enhancement, [Eu/Fe] $\leq +0.3$. Fig. 2 shows the abundance excess, which is the difference between the individual chemical abundance measurements in each star and the baseline abundance for that element. Three sets of elements behave similarly in our sample: Se, Sr, Y, Zr, Nb, and Mo ($34 \leq Z \leq 42$); Cd, Sn, and Te ($48 \leq Z \leq 52$); and Ba, La, Ce, Pr, Nd, and Sm ($56 \leq Z \leq 62$). They are grouped together in panels A, C, and D, respectively. Ratios among these elements exhibit no significant correlation with [Eu/Fe], and therefore no excess *(8)*.

Two sets of elements exhibit significant positive correlations with [Eu/Fe] *(8)*: Ru, Rh, Pd, and Ag ($44 \leq Z \leq 47$); and Gd, Tb, Dy, Ho, Er, Tm, Yb, Hf, Os, and Pt ($64 \leq Z \leq 78$; plus Eu, $Z = 63$). They are grouped together in panels B and E, respectively, of Fig. 2. These correlations signify a newly identified extension of r-process universality that links many of the heavier r-process elements with a few lighter ones. Previous work has shown that the range of elements that participate in universality is bounded by two important deviations (supplementary text). One is characterized by large (> 1.5 dex) differences in the overall amounts of lighter r-process elements (atomic numbers $34 \leq Z < 56$) relative to the heavier ($Z \geq 56$) ones. The other is characterized by small (< 0.7 dex) variations in the abundances of the actinide elements Th (Z = 90) and U (Z = 92) relative to other heavy r-process elements. Our findings also represent deviations from standard two-component models of r-process nucleosynthesis *(9, 10)*, where one component (a weak, or limited, r-process) is mainly responsible for the lighter r-process elements and another (a main r-process) is mainly responsible for the heavier r-process elements.

We propose that these element groups ($44 \leq Z \leq 47$ and $63 \leq Z \leq 78$) are coproduced as transuranic ($Z > 92$) fission fragments in the r-process, establishing a natural connection between them. Models predict that transuranic elements are produced in r-process events when the ejecta contain very neutron-rich material *(11–13)*. In these cases, the synthesis of heavy elements terminates when transuranic nuclei undergo fission and repopulate the r-process chain at lower masses *(14)*. Fission deposition effectively "washes away" variations in the initial conditions *(15)*, leading to robust relative abundances among the fission products, such as Ag and Eu. *(16)* recognized this behavior as a potential signature of fission, through a comparison of theoretical calculations with Pd, Ag, and Eu abundances in a limited sample of stars. This behavior can be seen in Fig. 3, which uses neutron star merger dynamical ejecta *(8)* to demonstrate the impact of fissioning on the log ε(Ag/Eu) ratios. Models that do not include a fission component (panel A) are sensitive to differences in initial conditions, such as progenitor mass, and they predict varying log ε(Ag/Eu) ratios in the ejecta. Additionally, neutron star merger dynamical ejecta is accompanied by ejecta from the post-merger accretion disk, which likely contains few or no fissioning nuclei, so additional ejecta from the disk could lead to even larger variations from one event to another. Models that include a fission component (panel B) predict that the mass-weighted log ε(Ag/Eu) ratios are approximately constant, and they match the observed stellar ratios. Similar behavior is expected for other candidate sites. For example, the neutron richness predicted for the ejecta of magneto-rotationally driven supernovae is known to vary based on the magnetic field of the progenitor *(17)*. In any site capable of hosting fission, fission deposition acts to stabilize the abundance ratios of coproduced elements against such astrophysical variations.

Figure 1 illustrates the feasibility of this proposed scenario. The green bands in Fig. 1 mark the baseline abundance pattern, which we calculate from the stars that we assume contain minimal contributions from fission deposition. We add contributions from transuranic fission fragments, enhanced by factors of 1, 2, and 4 relative to the baseline pattern *(8)*. These enhancement factors span the range of abundance excesses found for elements with $44 \leq Z \leq 47$ and $63 \leq Z \leq 78$ in the stars with the highest levels of [Eu/Fe], which are marked by the largest symbols in Fig. 1. Fission fragment deposition may contribute up to ≈ 75% of the production of the elements with the largest observed excesses, including Pd, Ag, Gd, and Yb *(8)*.

Substantial contributions from fission fragments of transuranic nuclei provide the most compelling explanation for the correlations between elements with with $44 \leq Z \leq 47$ and $63 \leq Z \leq 78$. No other known nucleosynthesis process, including the weak or main s-process, intermediate neutron-capture process, or weak r-process, can reproduce the observed behavior (supplementary text). This behavior is also not related to the actinide boost phenomenon that is observed in some r-process-enhanced stars (supplementary text, Fig. S3). It cautions against using [Ba/Eu] ratios to discern the presence of small amounts of s-process material in stars where the r-process contribution is dominant (supplementary text). The correlations are more closely associated with [Eu/Fe] than log ε(Eu) as a measure of the strength of the r-process (supplementary text), which suggests a link between r-process production of fissioning transuranic elements and the local environment.

Many of the radioactive, neutron-rich nuclei populated during the r-process are inaccessible to laboratory experiments, so theoretical models are necessary to estimate their properties. These models must be extrapolated from more stable isotopes located near the valley of stability. This extrapolation leads to large uncertainties in key quantities, such as masses, halflives, neutron-capture cross sections, and decay channels, which propagate into uncertainties in the abundance yields *(18)*. Our dataset provides new constraints on these models. For example, many of the fissioning nuclei influencing r-process abundances are predicted to have asymmetric distributions with a lighter peak and a heavier peak *(19)*. The lighter fragments are likely contributing to the Ru, Rh, Pd, and Ag abundances in these stars. Atomic mass numbers $99 \leq A \leq 110$ represent the stable isotopes of these elements that can be synthesized in the r-process, via β decays of the neutron-rich nuclei created directly through fission deposition. The heavier fragments likely contribute to the Eu and heavier elements ($A > 150$) in these stars. These mass ranges imply that nuclei with $A > 260$ (i.e., 110 + 150) are produced in the r-process and contribute substantially to the fission fragments. If the r-process synthesizes nuclei as heavy as $A \sim 280$, around the predicted nuclear shell closure at 184 neutrons *(13, 20)*, the heavier-mass fragments would include nuclei with $A > 170$ and encompass the lanthanide elements *(19, 21, 22)*. This prediction is consistent with our findings. Much larger samples of stars with a wide range of levels of r-process enhancement—and additional observations of Cd, Sn, Te, Hf, Os, and Pt in particular (supplementary text)—are needed to further constrain these model predictions.

The observational link between elements with $44 \leq Z \leq 47$ and $63 \leq Z \leq 78$ offers the strongest evidence yet for r-process production of nuclei with $A > 260$. Our findings boost the prospects for searches for the γ-rays associated with fission fragments *(23)* and efforts to assess how fissioning species impact the kilonova light curves associated with neutron star mergers *(24–26)*. They can motivate new theoretical efforts to determine whether superheavy elements are produced in the r-process *(27)*. Astronomical observations of fission fragments can help prioritize the most critical measurements of the properties of short-lived neutron-rich nuclei with the next generation of radioactive-isotope beam facilities *(28)*. This new line of inquiry can also complement and focus studies of the fission debris from the Trinity test *(29)* and other tests conducted on nuclear explosion debris *(30, 31)*, as well as studies of fission products extracted from the natural reactor located at Oklo, Gabon *(32)*. The fission products found in r-process-enhanced stars may even probe much heavier parent nuclei than ones accessible to these terrestrial sources. Our study highlights the importance of collecting new astronomical data in pursuit of this goal.

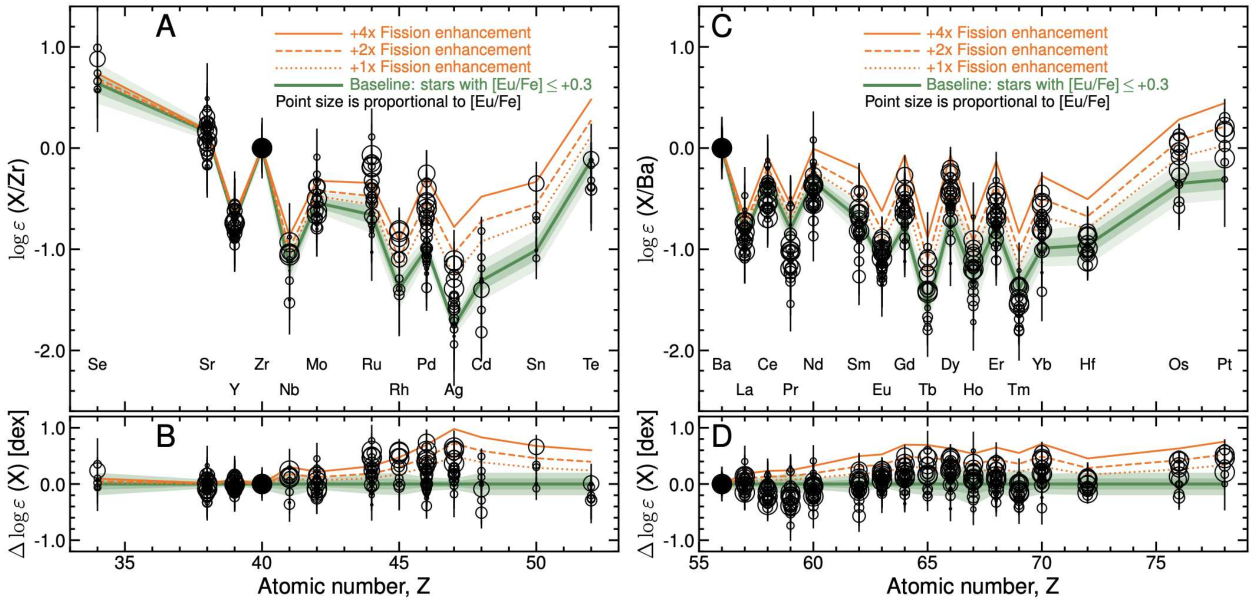

Fig. 1: Comparison between the observed abundance patterns and fission model predictions. The baseline pattern (green line) is defined as the mean ± 1 or 2 times the standard error (shaded green bands) of the abundance ratios in the stars with [Eu/Fe] ≤ +0.3. The orange curves illustrate fission fragments added to this baseline pattern; e.g., +2x enhancement means 2 parts fission fragments and 1 part baseline pattern. The size of each point is proportional to the [Eu/Fe] ratio in the star, as shown in Fig. 1. Panels **A** and **C** illustrate the log ε abundance ratios, defined as $\log_{10}(N_X/N_{Zr})$ or $\log_{10}(N_X/N_{Ba})$, where N_X, N_{Zr}, and N_{Ba} represent the number densities of elements X (for X = Se, Sr, ..., Te) and Zr or X (for X = La, Ce, ..., Pt) and Ba, respectively. Panels **B** and **D** illustrate the differences between each star or fission model and the baseline pattern.

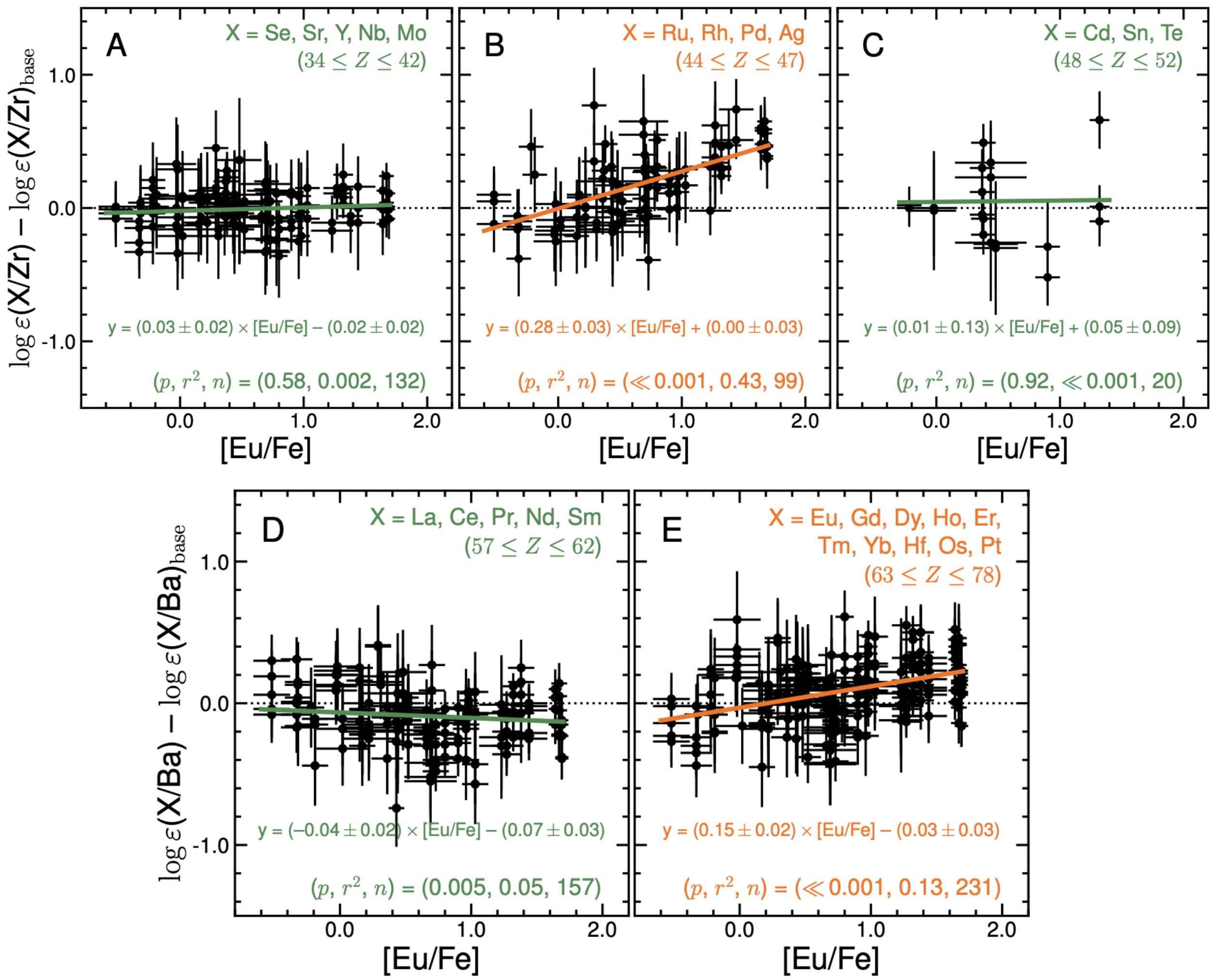

Fig. 2: Chemical abundance ratios for elements that exhibit no significant correlations with [Eu/Fe] (panels A, C, and D) and those that do (panels B and E). The panels are ordered by increasing atomic number, *Z*. Each point represents one ratio in one star, and the errorbars represent ± 1σ uncertainties. The log ε(X/Zr) and log ε(X/Ba) ratios are normalized to the baseline patterns, log ε(X/Zr)$_{\text{base}}$ and log ε(X/Ba)$_{\text{base}}$. The abundances of the lighter r-process elements ($34 \leq Z \leq 52$) are only partially correlated with the abundances of the heavier r-process elements ($56 \leq Z \leq 78$), so each group is normalized separately to Zr and Ba, respectively. Solid lines mark weighted least-squares linear fits, and the equations for these fits are printed in each panel. Dotted lines mark differences of zero. Flat trends (green lines) indicate that an element is coproduced with Zr or Ba, and significant correlations (orange lines) indicate that an element is

coproduced with Eu. The three values printed in the lower right corner of each panel list the *p*-value for the Pearson correlation coefficient, the r^2 coefficient of determination, and the number of stars, *n (8)*.

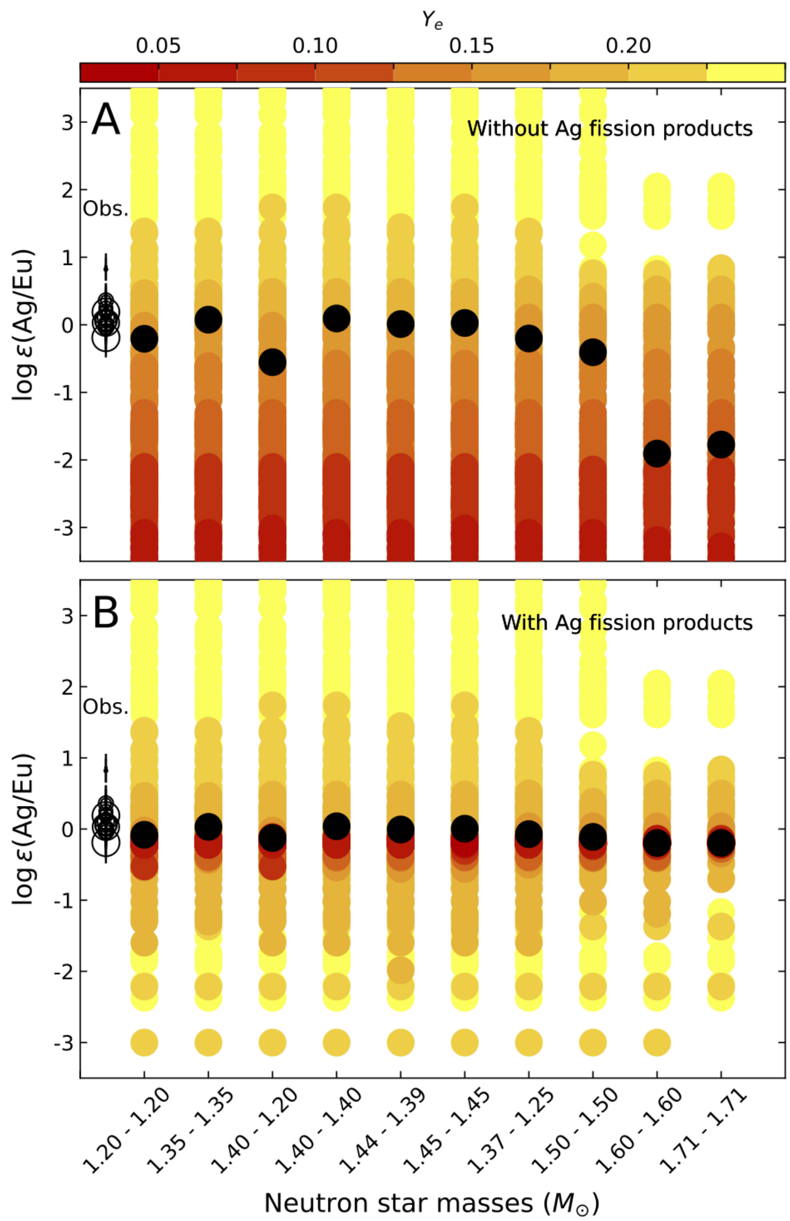

Fig. 3: The log ε(Ag/Eu) abundance ratio predicted when fission deposition contributes to Ag (panel B) and when it does not (panel A). Results from hydrodynamic simulations *(8)* for neutron star mergers with various progenitor masses are shown as colored dots for individual ejecta and black dots for the mass-weighted abundance ratio. Individual ejecta are colored based on their neutron richness, Y_e, with lower Y_e ejecta able to reach fissioning nuclei. When fission deposition contributes to Ag, the predicted mass-weighted log ε(Ag/Eu) ratios are independent of

the progenitor masses and match the observed ratios (black circles, whose size is proportional to the [Eu/Fe] ratio in each star).

References and notes

(1) B. P. Abbott, R. Abbott, T. D. Abbott, F. Acernese, K. Ackley, C. Adams, T. Adams, P. Addesso, R. X. Adhikari, V. B. Adya, C. Affeldt, M. Afrough, B. Agarwal, M. Agathos, K. Agatsuma, N. Aggarwal, O. D. Aguiar, L. Aiello, A. Ain, P. Ajith, B. Allen, G. Allen, A. Allocca, P. A. Altin, A. Amato, A. Ananyeva, S. B. Anderson, W. G. Anderson, S. V. Angelova, S. Antier, S. Appert, K. Arai, M. C. Araya, J. S. Areeda, N. Arnaud, K. G. Arun, S. Ascenzi, G. Ashton, M. Ast, S. M. Aston, P. Astone, D. V. Atallah, P. Aufmuth, C. Aulbert, K. AultONeal, C. Austin, A. Avila-Alvarez, S. Babak, P. Bacon, M. K. M. Bader, S. Bae, M. Bailes, P. T. Baker, F. Baldaccini, G. Ballardin, S. W. Ballmer, S. Banagiri, J. C. Barayoga, S. E. Barclay, B. C. Barish, D. Barker, K. Barkett, F. Barone, B. Barr, L. Barsotti, M. Barsuglia, D. Barta, S. D. Barthelmy, J. Bartlett, I. Bartos, R. Bassiri, A. Basti, J. C. Batch, M. Bawaj, J. C. Bayley, M. Bazzan, B. Bécsy, C. Beer, M. Bejger, I. Belahcene, A. S. Bell, B. K. Berger, G. Bergmann, S. Bernuzzi, J. J. Bero, C. P. L. Berry, D. Bersanetti, A. Bertolini, J. Betzwieser, S. Bhagwat, R. Bhandare, I. A. Bilenko, G. Billingsley, C. R. Billman, J. Birch, R. Birney, O. Birnholtz, S. Biscans, S. Biscoveanu, A. Bisht, M. Bitossi, C. Biwer, M. A. Bizouard, J. K. Blackburn, J. Blackman, C. D. Blair, D. G. Blair, R. M. Blair, S. Bloemen, O. Bock, N. Bode, M. Boer, G. Bogaert, A. Bohe, F. Bondu, E. Bonilla, R. Bonnand, B. A. Boom, R. Bork, V. Boschi, S. Bose, K. Bossie, Y. Bouffanais, A. Bozzi, C. Bradaschia, P. R. Brady, M. Branchesi, J. E. Brau, T. Briant, A. Brillet, M. Brinkmann, V. Brisson, P. Brockill, J. E. Broida, A. F. Brooks, D. A. Brown, D. D. Brown, S. Brunett, C. C. Buchanan, A. Buikema, T. Bulik, H. J. Bulten, A. Buonanno, D. Buskulic, C. Buy, R. L. Byer, M. Cabero, L. Cadonati, G. Cagnoli, C. Cahillane, J. Calderón Bustillo, T. A. Callister, E. Calloni, J. B. Camp, M. Canepa, P. Canizares, K. C.

Cannon, H. Cao, J. Cao, C. D. Capano, E. Capocasa, F. Carbognani, S. Caride, M. F. Carney, G. Carullo, J. Casanueva Diaz, C. Casentini, S. Caudill, M. Cavaglià, F. Cavalier, R. Cavalieri, G. Cella, C. B. Cepeda, P. Cerdá-Durán, G. Cerretani, E. Cesarini, S. J. Chamberlin, M. Chan, S. Chao, P. Charlton, E. Chase, E. Chassande-Mottin, D. Chatterjee, K. Chatziioannou, B. D. Cheeseboro, H. Y. Chen, X. Chen, Y. Chen, H. -P. Cheng, H. Chia, A. Chincarini, A. Chiummo, T. Chmiel, H. S. Cho, M. Cho, J. H. Chow, N. Christensen, Q. Chu, A. J. K. Chua, S. Chua, A. K. W. Chung, S. Chung, G. Ciani, R. Ciolfi, C. E. Cirelli, A. Cirone, F. Clara, J. A. Clark, P. Clearwater, F. Cleva, C. Cocchieri, E. Coccia, P. -F. Cohadon, D. Cohen, A. Colla, C. G. Collette, L. R. Cominsky, M. Constancio, L. Conti, S. J. Cooper, P. Corban, T. R. Corbitt, I. Cordero-Carrión, K. R. Corley, N. Cornish, A. Corsi, S. Cortese, C. A. Costa, M. W. Coughlin, S. B. Coughlin, J. -P. Coulon, S. T. Countryman, P. Couvares, P. B. Covas, E. E. Cowan, D. M. Coward, M. J. Cowart, D. C. Coyne, R. Coyne, J. D. E. Creighton, T. D. Creighton, J. Cripe, S. G. Crowder, T. J. Cullen, A. Cumming, L. Cunningham, E. Cuoco, T. Dal Canton, G. Dálya, S. L. Danilishin, S. D'Antonio, K. Danzmann, A. Dasgupta, C. F. Da Silva Costa, V. Dattilo, I. Dave, M. Davier, D. Davis, E. J. Daw, B. Day, S. De, D. DeBra, J. Degallaix, M. De Laurentis, S. Deléglise, W. Del Pozzo, N. Demos, T. Denker, T. Dent, R. De Pietri, V. Dergachev, R. De Rosa, R. T. DeRosa, C. De Rossi, R. DeSalvo, O. de Varona, J. Devenson, S. Dhurandhar, M. C. Díaz, T. Dietrich, L. Di Fiore, M. Di Giovanni, T. Di Girolamo, A. Di Lieto, S. Di Pace, I. Di Palma, F. Di Renzo, Z. Doctor, V. Dolique, F. Donovan, K. L. Dooley, S. Doravari, I. Dorrington, R. Douglas, M. Dovale Álvarez, T. P. Downes, M. Drago, C. Dreissigacker, J. C. Driggers, Z. Du, M. Ducrot, R. Dudi, P. Dupej, S. E. Dwyer, T. B. Edo, M. C. Edwards, A. Effler, H. -B. Eggenstein, P. Ehrens, J. Eichholz, S. S. Eikenberry, R. A. Eisenstein, R. C. Essick, D. Estevez, Z. B. Etienne, T. Etzel, M. Evans, T. M. Evans, M. Factourovich, V. Fafone, H. Fair, S. Fairhurst, X. Fan, S. Farinon, B. Farr, W. M. Farr, E. J. Fauchon-Jones, M. Favata, M.

Fays, C. Fee, H. Fehrmann, J. Feicht, M. M. Fejer, A. Fernandez-Galiana, I. Ferrante, E. C. Ferreira, F. Ferrini, F. Fidecaro, D. Finstad, I. Fiori, D. Fiorucci, M. Fishbach, R. P. Fisher, M. Fitz-Axen, R. Flaminio, M. Fletcher, H. Fong, J. A. Font, P. W. F. Forsyth, S. S. Forsyth, J. -D. Fournier, S. Frasca, F. Frasconi, Z. Frei, A. Freise, R. Frey, V. Frey, E. M. Fries, P. Fritschel, V. V. Frolov, P. Fulda, M. Fyffe, H. Gabbard, B. U. Gadre, S. M. Gaebel, J. R. Gair, L. Gammaitoni, M. R. Ganija, S. G. Gaonkar, C. Garcia-Quiros, F. Garufi, B. Gateley, S. Gaudio, G. Gaur, V. Gayathri, N. Gehrels, G. Gemme, E. Genin, A. Gennai, D. George, J. George, L. Gergely, V. Germain, S. Ghonge, Abhirup Ghosh, Archisman Ghosh, S. Ghosh, J. A. Giaime, K. D. Giardina, A. Giazotto, K. Gill, L. Glover, E. Goetz, R. Goetz, S. Gomes, B. Goncharov, G. González, J. M. Gonzalez Castro, A. Gopakumar, M. L. Gorodetsky, S. E. Gossan, M. Gosselin, R. Gouaty, A. Grado, C. Graef, M. Granata, A. Grant, S. Gras, C. Gray, G. Greco, A. C. Green, E. M. Gretarsson, P. Groot, H. Grote, S. Grunewald, P. Gruning, G. M. Guidi, X. Guo, A. Gupta, M. K. Gupta, K. E. Gushwa, E. K. Gustafson, R. Gustafson, O. Halim, B. R. Hall, E. D. Hall, E. Z. Hamilton, G. Hammond, M. Haney, M. M. Hanke, J. Hanks, C. Hanna, M. D. Hannam, O. A. Hannuksela, J. Hanson, T. Hardwick, J. Harms, G. M. Harry, I. W. Harry, M. J. Hart, C. -J. Haster, K. Haughian, J. Healy, A. Heidmann, M. C. Heintze, H. Heitmann, P. Hello, G. Hemming, M. Hendry, I. S. Heng, J. Hennig, A. W. Heptonstall, M. Heurs, S. Hild, T. Hinderer, W. C. G. Ho, D. Hoak, D. Hofman, K. Holt, D. E. Holz, P. Hopkins, C. Horst, J. Hough, E. A. Houston, E. J. Howell, A. Hreibi, Y. M. Hu, E. A. Huerta, D. Huet, B. Hughey, S. Husa, S. H. Huttner, T. Huynh-Dinh, N. Indik, R. Inta, G. Intini, H. N. Isa, J. -M. Isac, M. Isi, B. R. Iyer, K. Izumi, T. Jacqmin, K. Jani, P. Jaranowski, S. Jawahar, F. Jiménez-Forteza, W. W. Johnson, N. K. Johnson-McDaniel, D. I. Jones, R. Jones, R. J. G. Jonker, L. Ju, J. Junker, C. V. Kalaghatgi, V. Kalogera, B. Kamai, S. Kandhasamy, G. Kang, J. B. Kanner, S. J. Kapadia, S. Karki, K. S. Karvinen, M. Kasprzack, W. Kastaun, M. Katolik, E. Katsavounidis, W. Katzman, S. Kaufer, K.

Kawabe, F. Kéfélian, D. Keitel, A. J. Kemball, R. Kennedy, C. Kent, J. S. Key, F. Y. Khalili, I. Khan, S. Khan, Z. Khan, E. A. Khazanov, N. Kijbunchoo, Chunglee Kim, J. C. Kim, K. Kim, W. Kim, W. S. Kim, Y. -M. Kim, S. J. Kimbrell, E. J. King, P. J. King, M. Kinley-Hanlon, R. Kirchhoff, J. S. Kissel, L. Kleybolte, S. Klimenko, T. D. Knowles, P. Koch, S. M. Koehlenbeck, S. Koley, V. Kondrashov, A. Kontos, M. Korobko, W. Z. Korth, I. Kowalska, D. B. Kozak, C. Krämer, V. Kringel, B. Krishnan, A. Królak, G. Kuehn, P. Kumar, R. Kumar, S. Kumar, L. Kuo, A. Kutynia, S. Kwang, B. D. Lackey, K. H. Lai, M. Landry, R. N. Lang, J. Lange, B. Lantz, R. K. Lanza, S. L. Larson, A. Lartaux-Vollard, P. D. Lasky, M. Laxen, A. Lazzarini, C. Lazzaro, P. Leaci, S. Leavey, C. H. Lee, H. K. Lee, H. M. Lee, H. W. Lee, K. Lee, J. Lehmann, A. Lenon, E. Leon, M. Leonardi, N. Leroy, N. Letendre, Y. Levin, T. G. F. Li, S. D. Linker, T. B. Littenberg, J. Liu, X. Liu, R. K. L. Lo, N. A. Lockerbie, L. T. London, J. E. Lord, M. Lorenzini, V. Loriette, M. Lormand, G. Losurdo, J. D. Lough, C. O. Lousto, G. Lovelace, H. Lück, D. Lumaca, A. P. Lundgren, R. Lynch, Y. Ma, R. Macas, S. Macfoy, B. Machenschalk, M. MacInnis, D. M. Macleod, I. Magaña Hernandez, F. Magaña-Sandoval, L. Magaña Zertuche, R. M. Magee, E. Majorana, I. Maksimovic, N. Man, V. Mandic, V. Mangano, G. L. Mansell, M. Manske, M. Mantovani, F. Marchesoni, F. Marion, S. Márka, Z. Márka, C. Markakis, A. S. Markosyan, A. Markowitz, E. Maros, A. Marquina, P. Marsh, F. Martelli, L. Martellini, I. W. Martin, R. M. Martin, D. V. Martynov, J. N. Marx, K. Mason, E. Massera, A. Masserot, T. J. Massinger, M. Masso-Reid, S. Mastrogiovanni, A. Matas, F. Matichard, L. Matone, N. Mavalvala, N. Mazumder, R. McCarthy, D. E. McClelland, S. McCormick, L. McCuller, S. C. McGuire, G. McIntyre, J. McIver, D. J. McManus, L. McNeill, T. McRae, S. T. McWilliams, D. Meacher, G. D. Meadors, M. Mehmet, J. Meidam, E. Mejuto-Villa, A. Melatos, G. Mendell, R. A. Mercer, E. L. Merilh, M. Merzougui, S. Meshkov, C. Messenger, C. Messick, R. Metzdorff, P. M. Meyers, H. Miao, C. Michel, H. Middleton, E. E. Mikhailov, L. Milano, A. L. Miller, B. B. Miller, J.

Miller, M. Millhouse, M. C. Milovich-Goff, O. Minazzoli, Y. Minenkov, J. Ming, C. Mishra, S. Mitra, V. P. Mitrofanov, G. Mitselmakher, R. Mittleman, D. Moffa, A. Moggi, K. Mogushi, M. Mohan, S. R. P. Mohapatra, I. Molina, M. Montani, C. J. Moore, D. Moraru, G. Moreno, S. Morisaki, S. R. Morriss, B. Mours, C. M. Mow-Lowry, G. Mueller, A. W. Muir, Arunava Mukherjee, D. Mukherjee, S. Mukherjee, N. Mukund, A. Mullavey, J. Munch, E. A. Muñiz, M. Muratore, P. G. Murray, A. Nagar, K. Napier, I. Nardecchia, L. Naticchioni, R. K. Nayak, J. Neilson, G. Nelemans, T. J. N. Nelson, M. Nery, A. Neunzert, L. Nevin, J. M. Newport, G. Newton, K. K. Y. Ng, P. Nguyen, T. T. Nguyen, D. Nichols, A. B. Nielsen, S. Nissanke, A. Nitz, A. Noack, F. Nocera, D. Nolting, C. North, L. K. Nuttall, J. Oberling, G. D. O'Dea, G. H. Ogin, J. J. Oh, S. H. Oh, F. Ohme, M. A. Okada, M. Oliver, P. Oppermann, Richard J. Oram, B. O'Reilly, R. Ormiston, L. F. Ortega, R. O'Shaughnessy, S. Ossokine, D. J. Ottaway, H. Overmier, B. J. Owen, A. E. Pace, J. Page, M. A. Page, A. Pai, S. A. Pai, J. R. Palamos, O. Palashov, C. Palomba, A. Pal-Singh, Howard Pan, Huang-Wei Pan, B. Pang, P. T. H. Pang, C. Pankow, F. Pannarale, B. C. Pant, F. Paoletti, A. Paoli, M. A. Papa, A. Parida, W. Parker, D. Pascucci, A. Pasqualetti, R. Passaquieti, D. Passuello, M. Patil, B. Patricelli, B. L. Pearlstone, M. Pedraza, R. Pedurand, L. Pekowsky, A. Pele, S. Penn, C. J. Perez, A. Perreca, L. M. Perri, H. P. Pfeiffer, M. Phelps, O. J. Piccinni, M. Pichot, F. Piergiovanni, V. Pierro, G. Pillant, L. Pinard, I. M. Pinto, M. Pirello, M. Pitkin, M. Poe, R. Poggiani, P. Popolizio, E. K. Porter, A. Post, J. Powell, J. Prasad, J. W. W. Pratt, G. Pratten, V. Predoi, T. Prestegard, M. Prijatelj, M. Principe, S. Privitera, R. Prix, G. A. Prodi, L. G. Prokhorov, O. Puncken, M. Punturo, P. Puppo, M. Pürrer, H. Qi, V. Quetschke, E. A. Quintero, R. Quitzow-James, F. J. Raab, D. S. Rabeling, H. Radkins, P. Raffai, S. Raja, C. Rajan, B. Rajbhandari, M. Rakhmanov, K. E. Ramirez, A. Ramos-Buades, P. Rapagnani, V. Raymond, M. Razzano, J. Read, T. Regimbau, L. Rei, S. Reid, D. H. Reitze, W. Ren, S. D. Reyes, F. Ricci, P. M. Ricker, S. Rieger, K. Riles, M. Rizzo, N. A. Robertson, R.

Robie, F. Robinet, A. Rocchi, L. Rolland, J. G. Rollins, V. J. Roma, J. D. Romano, R. Romano, C. L. Romel, J. H. Romie, D. Rosińska, M. P. Ross, S. Rowan, A. Rüdiger, P. Ruggi, G. Rutins, K. Ryan, S. Sachdev, T. Sadecki, L. Sadeghian, M. Sakellariadou, L. Salconi, M. Saleem, F. Salemi, A. Samajdar, L. Sammut, L. M. Sampson, E. J. Sanchez, L. E. Sanchez, N. Sanchis-Gual, V. Sandberg, J. R. Sanders, B. Sassolas, B. S. Sathyaprakash, P. R. Saulson, O. Sauter, R. L. Savage, A. Sawadsky, P. Schale, M. Scheel, J. Scheuer, J. Schmidt, P. Schmidt, R. Schnabel, R. M. S. Schofield, A. Schönbeck, E. Schreiber, D. Schuette, B. W. Schulte, B. F. Schutz, S. G. Schwalbe, J. Scott, S. M. Scott, E. Seidel, D. Sellers, A. S. Sengupta, D. Sentenac, V. Sequino, A. Sergeev, D. A. Shaddock, T. J. Shaffer, A. A. Shah, M. S. Shahriar, M. B. Shaner, L. Shao, B. Shapiro, P. Shawhan, A. Sheperd, D. H. Shoemaker, D. M. Shoemaker, K. Siellez, X. Siemens, M. Sieniawska, D. Sigg, A. D. Silva, L. P. Singer, A. Singh, A. Singhal, A. M. Sintes, B. J. J. Slagmolen, B. Smith, J. R. Smith, R. J. E. Smith, S. Somala, E. J. Son, J. A. Sonnenberg, B. Sorazu, F. Sorrentino, T. Souradeep, A. P. Spencer, A. K. Srivastava, K. Staats, A. Staley, M. Steinke, J. Steinlechner, S. Steinlechner, D. Steinmeyer, S. P. Stevenson, R. Stone, D. J. Stops, K. A. Strain, G. Stratta, S. E. Strigin, A. Strunk, R. Sturani, A. L. Stuver, T. Z. Summerscales, L. Sun, S. Sunil, J. Suresh, P. J. Sutton, B. L. Swinkels, M. J. Szczepańczyk, M. Tacca, S. C. Tait, C. Talbot, D. Talukder, D. B. Tanner, M. Tápai, A. Taracchini, J. D. Tasson, J. A. Taylor, R. Taylor, S. V. Tewari, T. Theeg, F. Thies, E. G. Thomas, M. Thomas, P. Thomas, K. A. Thorne, K. S. Thorne, E. Thrane, S. Tiwari, V. Tiwari, K. V. Tokmakov, K. Toland, M. Tonelli, Z. Tornasi, A. Torres-Forné, C. I. Torrie, D. Töyrä, F. Travasso, G. Traylor, J. Trinastic, M. C. Tringali, L. Trozzo, K. W. Tsang, M. Tse, R. Tso, L. Tsukada, D. Tsuna, D. Tuyenbayev, K. Ueno, D. Ugolini, C. S. Unnikrishnan, A. L. Urban, S. A. Usman, H. Vahlbruch, G. Vajente, G. Valdes, M. Vallisneri, N. van Bakel, M. van Beuzekom, J. F. J. van den Brand, C. Van Den Broeck, D. C. Vander-Hyde, L. van der Schaaf, J. V. van Heijningen, A. A. van Veggel, M.

Vardaro, V. Varma, S. Vass, M. Vasúth, A. Vecchio, G. Vedovato, J. Veitch, P. J. Veitch, K. Venkateswara, G. Venugopalan, D. Verkindt, F. Vetrano, A. Viceré, A. D. Viets, S. Vinciguerra, D. J. Vine, J. -Y. Vinet, S. Vitale, T. Vo, H. Vocca, C. Vorvick, S. P. Vyatchanin, A. R. Wade, L. E. Wade, M. Wade, R. Walet, M. Walker, L. Wallace, S. Walsh, G. Wang, H. Wang, J. Z. Wang, W. H. Wang, Y. F. Wang, R. L. Ward, J. Warner, M. Was, J. Watchi, B. Weaver, L. -W. Wei, M. Weinert, A. J. Weinstein, R. Weiss, L. Wen, E. K. Wessel, P. Weßels, J. Westerweck, T. Westphal, K. Wette, J. T. Whelan, S. E. Whitcomb, B. F. Whiting, C. Whittle, D. Wilken, D. Williams, R. D. Williams, A. R. Williamson, J. L. Willis, B. Willke, M. H. Wimmer, W. Winkler, C. C. Wipf, H. Wittel, G. Woan, J. Woehler, J. Wofford, K. W. K. Wong, J. Worden, J. L. Wright, D. S. Wu, D. M. Wysocki, S. Xiao, H. Yamamoto, C. C. Yancey, L. Yang, M. J. Yap, M. Yazback, Hang Yu, Haocun Yu, M. Yvert, A. ZadroŻny, M. Zanolin, T. Zelenova, J. -P. Zendri, M. Zevin, L. Zhang, M. Zhang, T. Zhang, Y. -H. Zhang, C. Zhao, M. Zhou, Z. Zhou, S. J. Zhu, X. J. Zhu, A. B. Zimmerman, M. E. Zucker, J. Zweizig, LIGO Scientific Collaboration, Virgo Collaboration. GW170817: Observation of Gravitational Waves from a Binary Neutron Star Inspiral. *Physical Review Letters* **119**, 161101 (2017).

(2) M. M. Kasliwal, E. Nakar, L. P. Singer, D. L. Kaplan, D. O. Cook, A. Van Sistine, R. M. Lau, C. Fremling, O. Gottlieb, J. E. Jencson, S. M. Adams, U. Feindt, K. Hotokezaka, S. Ghosh, D. A. Perley, P. -C. Yu, T. Piran, J. R. Allison, G. C. Anupama, A. Balasubramanian, K. W. Bannister, J. Bally, J. Barnes, S. Barway, E. Bellm, V. Bhalerao, D. Bhattacharya, N. Blagorodnova, J. S. Bloom, P. R. Brady, C. Cannella, D. Chatterjee, S. B. Cenko, B. E. Cobb, C. Copperwheat, A. Corsi, K. De, D. Dobie, S. W. K. Emery, P. A. Evans, O. D. Fox, D. A. Frail, C. Frohmaier, A. Goobar, G. Hallinan, F. Harrison, G. Helou, T. Hinderer, A. Y. Q. Ho, A. Horesh, W. -H. Ip, R. Itoh, D. Kasen, H. Kim, N. P. M. Kuin, T. Kupfer, C. Lynch, K. Madsen,

P. A. Mazzali, A. A. Miller, K. Mooley, T. Murphy, C. -C. Ngeow, D. Nichols, S. Nissanke, P. Nugent, E. O. Ofek, H. Qi, R. M. Quimby, S. Rosswog, F. Rusu, E. M. Sadler, P. Schmidt, J. Sollerman, I. Steele, A. R. Williamson, Y. Xu, L. Yan, Y. Yatsu, C. Zhang, W. Zhao. Illuminating gravitational waves: A concordant picture of photons from a neutron star merger. *Science* **358**, 1559-1565 (2017).

(3) M. W. Coughlin, T. Dietrich, Z. Doctor, D. Kasen, S. Coughlin, A. Jerkstrand, G. Leloudas, O. McBrien, B. D. Metzger, R. O'Shaughnessy, S. J. Smartt. Constraints on the neutron star equation of state from AT2017gfo using radiative transfer simulations. *Monthly Notices of the Royal Astronomical Society* **480**, 3871-3878 (2018).

(4) M. R. Drout, A. L. Piro, B. J. Shappee, C. D. Kilpatrick, J. D. Simon, C. Contreras, D. A. Coulter, R. J. Foley, M. R. Siebert, N. Morrell, K. Boutsia, F. Di Mille, T. W. -S. Holoien, D. Kasen, J. A. Kollmeier, B. F. Madore, A. J. Monson, A. Murguia-Berthier, Y. -C. Pan, J. X. Prochaska, E. Ramirez-Ruiz, A. Rest, C. Adams, K. Alatalo, E. Bañados, J. Baughman, T. C. Beers, R. A. Bernstein, T. Bitsakis, A. Campillay, T. T. Hansen, C. R. Higgs, A. P. Ji, G. Maravelias, J. L. Marshall, C. Moni Bidin, J. L. Prieto, K. C. Rasmussen, C. Rojas-Bravo, A. L. Strom, N. Ulloa, J. Vargas-González, Z. Wan, D. D. Whitten. Light curves of the neutron star merger GW170817/SSS17a: Implications for r-process nucleosynthesis. *Science* **358**, 1570-1574 (2017).

(5) D. Kasen, B. Metzger, J. Barnes, E. Quataert, E. Ramirez-Ruiz. Origin of the heavy elements in binary neutron-star mergers from a gravitational-wave event. *Nature* **551**, 80-84 (2017).

(6) D. Watson, C. J. Hansen, J. Selsing, A. Koch, D. B. Malesani, A. C. Andersen, J. P. U. Fynbo, A. Arcones, A. Bauswein, S. Covino, A. Grado, K. E. Heintz, L. Hunt, C. Kouveliotou, G. Leloudas, A. J. Levan, P. Mazzali, E. Pian. Identification of strontium in the merger of two neutron stars. *Nature* **574**, 497-500 (2019).

(7) J. J. Cowan, C. Sneden, J. E. Lawler, A. Aprahamian, M. Wiescher, K. Langanke, G. Martínez-Pinedo, F.-K. Thielemann. Origin of the heaviest elements: The rapid neutron-capture process. *Reviews of Modern Physics* **93**, 015002 (2021).

(8) Materials and methods are available as supplementary materials at the Science website.

(9) F. Montes, T. C. Beers, J. Cowan, T. Elliot, K. Farouqi, R. Gallino, M. Heil, K.-L. Kratz, B. Pfeiffer, M. Pignatari, H. Schatz. Nucleosynthesis in the early Galaxy. *The Astrophysical Journal* **671**, 1685-1695 (2007).

(10) Y.-Z. Qian, G. J. Wasserburg. Abundances of Sr, Y, and Zr in metal-poor stars and implications for chemical evolution in the early Galaxy. *The Astrophysical Journal* **687**, 272-286 (2008).

(11) S. Wanajo, Y. Sekiguchi, N. Nishimura, K. Kiuchi, K. Kyutoku, M. Shibata. Production of all the r-process nuclides in the dynamical ejecta of neutron star mergers. *The Astrophysical Journal* **789**, L39 (2014).

(12) M. Eichler, A. Arcones, A. Kelic, O. Korobkin, K. Langanke, T. Marketin, G. Martinez-Pinedo, I. Panov, T. Rauscher, S. Rosswog, C. Winteler, N. T. Zinner, F.-K. Thielemann. The role of fission in neutron star mergers and its impact on the r-process peaks. *The Astrophysical Journal* **808**, 30 (2015).

(13) S. Goriely, G. Martínez Pinedo. The production of transuranium elements by the r-process nucleosynthesis. *Nuclear Physics A* **944**, 158-176 (2015).

(14) I. V. Panov, I. Y. Korneev, F.-K. Thielemann. The r-Process in the region of transuranium elements and the contribution of fission products to the nucleosynthesis of nuclei with A ≤ 130. *Astronomy Letters* **34**, 189-197 (2008).

(15) T. M. Sprouse, R. Navarro Perez, R. Surman, M. R. Mumpower, G. C. McLaughlin, N. Schunck. Propagation of statistical uncertainties of Skyrme mass models to simulations of r-process nucleosynthesis. *Physical Review C* **101**, 055803 (2020).

(16) N. Vassh, M. R. Mumpower, G. C. McLaughlin, T. M. Sprouse, R. Surman. Coproduction of light and heavy r-process elements via fission deposition. *The Astrophysical Journal* **896**, 28 (2020).

(17) M. Reichert, M. Obergaulinger, M. Eichler, M. Á. Aloy, A. Arcones. Nucleosynthesis in magneto-rotational supernovae. *Monthly Notices of the Royal Astronomical Society* **501**, 5733-5745 (2021).

(18) M. R. Mumpower, R. Surman, G. C. McLaughlin, A. Aprahamian. The impact of individual nuclear properties on r-process nucleosynthesis. *Progress in Particle and Nuclear Physics* **86**, 86-126 (2016).

(19) J.-F. Lemaître, S. Goriely, A. Bauswein, H.-T. Janka. Fission fragment distributions and their impact on the r -process nucleosynthesis in neutron star mergers. *Physical Review C* **103**, 025806 (2021).

(20) H. Schatz, R. Toenjes, B. Pfeiffer, T. C. Beers, J. J. Cowan, V. Hill, K.-L. Kratz. Thorium and uranium chronometers applied to CS 31082-001. *The Astrophysical Journal* **579**, 626-638 (2002).

(21) J. Beun, G. C. McLaughlin, R. Surman, W. R. Hix. Fission cycling in a supernova r process. *Physical Review C* **77**, 035804 (2008).

(22) S. Goriely, J.-L. Sida, J.-F. Lemaître, S. Panebianco, N. Dubray, S. Hilaire, A. Bauswein, H.-T. Janka. New fission fragment distributions and r-process origin of the rare-earth elements. *Physical Review Letters* **111**, 242502 (2013).

(23) X. Wang, N3AS Collaboration, N. Vassh, FIRE Collaboration, T. Sprouse, M. Mumpower, R. Vogt, J. Randrup, R. Surman. MeV gamma rays from fission: A distinct signature of actinide production in neutron star mergers. *The Astrophysical Journal* **903**, L3 (2020).

(24) S. Wanajo. Physical conditions for the r-process. I. Radioactive energy sources of kilonovae. *The Astrophysical Journal* **868**, 65 (2018).

(25) Y. Zhu, R. T. Wollaeger, N. Vassh, R. Surman, T. M. Sprouse, M. R. Mumpower, P. Möller, G. C. McLaughlin, O. Korobkin, T. Kawano, P. J. Jaffke, E. M. Holmbeck, C. L. Fryer, W. P. Even, A. J. Couture, J. Barnes. Californium-254 and kilonova light curves. *The Astrophysical Journal* **863**, L23 (2018).

(26) M.-R. Wu, J. Barnes, G. Martínez-Pinedo, B. D. Metzger. Fingerprints of heavy-element nucleosynthesis in the late-time lightcurves of kilonovae. *Physical Review Letters* **122**, 062701 (2019).

(27) I. Petermann, K. Langanke, G. Martínez-Pinedo, I. V. Panov, P.-G. Reinhard, F.-K. Thielemann. Have superheavy elements been produced in nature? *European Physical Journal A* **48**, 122 (2012).

(28) C. J. Horowitz, A. Arcones, B. Côté, I. Dillmann, W. Nazarewicz, I. U. Roederer, H. Schatz, A. Aprahamian, D. Atanasov, A. Bauswein, T. C. Beers, J. Bliss, M. Brodeur, J. A. Clark, A. Frebel, F. Foucart, C. J. Hansen, O. Just, A. Kankainen, G. C. McLaughlin, J. M. Kelly, S. N. Liddick, D. M. Lee, J. Lippuner, D. Martin, J. Mendoza-Temis, B. D. Metzger, M. R. Mumpower, G. Perdikakis, J. Pereira, B. W. O'Shea, R. Reifarth, A. M. Rogers, D. M. Siegel, A. Spyrou, R. Surman, X. Tang, T. Uesaka, M. Wang. R-process nucleosynthesis: connecting rare-isotope beam facilities with the cosmos. *Journal of Physics G Nuclear Physics* **46**, 083001 (2019).

(29) S. K. Hanson, A. D. Pollington, C. R. Waidmann, W. S. Kinman, A. M. Wende, J. L. Miller, J. A. Berger, W. J. Oldham, H. D. Selby. Measurements of extinct fission products in nuclear bomb debris: Determination of the yield of the Trinity nuclear test 70 y later. *Proceedings of the National Academy of Sciences* **113**, 8104-8108 (2016).

(30) S. A. Becker. Approximating the r-process on earth with thermonuclear explosions: Lessons learned and unanswered questions. *Origin and Evolution of the Elements*, Carnegie Observatories Astrophysics Series, Pasadena: Carnegie Observatories **4** (2004).

(31) A. Aprahamian. Open challenges to nuclear physics resulting from the neutron star merger. *Nuclear Physics News* **3**, 11-16 (2021).

(32) R. D. Loss, J. R. De Laeter, K. J. R. Rosman, T. M. Benjamin, D. B. Curtis, A. J. Gancarz, J. E. Delmore, W. J. Maeck. The Oklo natural reactors: cumulative fission yields and nuclear characteristics of Reactor Zone 9. *Earth and Planetary Science Letters* **89**, 193-206 (1988).

(33) A. Abohalima, A. Frebel. JINAbase—A database for chemical abundances of metal-poor stars. *The Astrophysical Journal Supplement Series* **238**, 36 (2018).

(34) A. Frebel. From nuclei to the cosmos: Tracing heavy-element production with the oldest stars. *Annual Review of Nuclear and Particle Science* **68**, 237-269 (2018).

(35) V. Hill, B. Plez, R. Cayrel, T. C. Beers, B. Nordström, J. Andersen, M. Spite, F. Spite, B. Barbuy, P. Bonifacio, E. Depagne, P. François, F. Primas. First stars. I. The extreme r-element rich, iron-poor halo giant CS 31082-001. Implications for the r-process site(s) and radioactive cosmochronology. *Astronomy and Astrophysics* **387**, 560-579 (2002).

(36) B. Barbuy, M. Spite, V. Hill, F. Primas, B. Plez, R. Cayrel, F. Spite, S. Wanajo, C. Siqueira Mello, J. Andersen, B. Nordström, T. C. Beers, P. Bonifacio, P. François, P. Molaro. First stars. XV. Third-peak r-process element and actinide abundances in the uranium-rich star CS31082-001. *Astronomy and Astrophysics* **534**, A60 (2011).

(37) C. Sneden, J. E. Lawler, J. J. Cowan, I. I. Ivans, E. A. Den Hartog. New rare earth element abundance distributions for the Sun and five r-process-rich very metal-poor stars. *The Astrophysical Journal Supplement Series* **182**, 80-96 (2009).

(38) C. Siqueira Mello, M. Spite, B. Barbuy, F. Spite, E. Caffau, V. Hill, S. Wanajo, F. Primas, B. Plez, R. Cayrel, J. Andersen, B. Nordström, C. Sneden, T. C. Beers, P. Bonifacio, P. François, P. Molaro. First stars. XVI. HST/STIS abundances of heavy elements in the uranium-rich metal-poor star CS 31082-001. *Astronomy and Astrophysics* **550**, A122 (2013).

(39) V. Hill, N. Christlieb, T. C. Beers, P. S. Barklem, K.-L. Kratz, B. Nordström, B. Pfeiffer, K. Farouqi. The Hamburg/ESO R-process Enhanced Star survey (HERES). XI. The highly r-process-enhanced star CS 29497-004. *Astronomy and Astrophysics* **607**, A91 (2017).

(40) C. Sneden, J. J. Cowan, J. E. Lawler, I. I. Ivans, S. Burles, T. C. Beers, F. Primas, V. Hill, J. W. Truran, G. M. Fuller, B. Pfeiffer, K.-L. Kratz. The extremely metal-poor, neutron capture-rich star CS 22892-052: A comprehensive abundance analysis. *The Astrophysical Journal* **591**, 936-953 (2003).

(41) J. J. Cowan, C. Sneden, T. C. Beers, J. E. Lawler, J. Simmerer, J. W. Truran, F. Primas, J. Collier, S. Burles. Hubble Space Telescope observations of heavy elements in metal-poor Galactic halo stars. *The Astrophysical Journal* **627**, 238-250 (2005).

(42) H. Nilsson, H. Hartman, L. Engström, H. Lundberg, C. Sneden, V. Fivet, P. Palmeri, P. Quinet, É. Biémont. Transition probabilities of astrophysical interest in the niobium ions Nb^{+} and Nb^{2+}. *Astronomy and Astrophysics* **511**, A16 (2010).

(43) M. Cain, A. Frebel, M. Gull, A. P. Ji, V. M. Placco, T. C. Beers, J. Meléndez, R. Ezzeddine, A. R. Casey, T. T. Hansen, I. U. Roederer, C. Sakari. The R-Process Alliance: Chemical abundances for a trio of r-process-enhanced Stars—one strong, one moderate, and one mild. *The Astrophysical Journal* **864**, 43 (2018).

(44) W. Hayek, U. Wiesendahl, N. Christlieb, K. Eriksson, A. J. Korn, P. S. Barklem, V. Hill, T. C. Beers, K. Farouqi, B. Pfeiffer, K.-L. Kratz. The Hamburg/ESO R-process enhanced star survey (HERES). IV. Detailed abundance analysis and age dating of the strongly r-process enhanced stars CS 29491-069 and HE 1219-0312. *Astronomy and Astrophysics* **504**, 511-524 (2009).

(45) I. U. Roederer, C. M. Sakari, V. M. Placco, T. C. Beers, R. Ezzeddine, A. Frebel, T. T. Hansen. The R-Process Alliance: A comprehensive abundance analysis of HD 222925, a metal-poor star with an extreme r-process enhancement of [Eu/H] = -0.14. *The Astrophysical Journal* **865**, 129 (2018).

(46) I. U. Roederer, J. E. Lawler, E. A. Den Hartog, V. M. Placco, R. Surman, T. C. Beers, R. Ezzeddine, A. Frebel, T. T. Hansen, K. Hattori, E. M. Holmbeck, C. M. Sakari. The R-process Alliance: A nearly complete r-process abundance template derived from ultraviolet spectroscopy of the r-process-enhanced metal-poor Star HD 222925. *The Astrophysical Journal Supplement Series* **260**, 27 (2022).

(47) C. M. Sakari, V. M. Placco, T. Hansen, E. M. Holmbeck, T. C. Beers, A. Frebel, I. U. Roederer, K. A. Venn, G. Wallerstein, C. E. Davis, E. M. Farrell, D. Yong. The r-process pattern of a bright, highly r-process-enhanced metal-poor halo star at [Fe/H] ~ −2. *The Astrophysical Journal* **854**, L20 (2018).

(48) D. K. Lai, M. Bolte, J. A. Johnson, S. Lucatello, A. Heger, S. E. Woosley. Detailed abundances for 28 metal-poor stars: Stellar relics in the Milky Way. *The Astrophysical Journal* **681**, 1524-1556 (2008).

(49) P. François, E. Depagne, V. Hill, M. Spite, F. Spite, B. Plez, T. C. Beers, J. Andersen, G. James, B. Barbuy, R. Cayrel, P. Bonifacio, P. Molaro, B. Nordström, F. Primas. First stars. VIII. Enrichment of the neutron-capture elements in the early Galaxy. *Astronomy and Astrophysics* **476**, 935-950 (2007).

(50) F. Spite, M. Spite, B. Barbuy, P. Bonifacio, E. Caffau, P. François. Abundance patterns of the light neutron-capture elements in very and extremely metal-poor stars. *Astronomy and Astrophysics* **611**, A30 (2018).

(51) L. Mashonkina, N. Christlieb, P. S. Barklem, V. Hill, T. C. Beers, A. Velichko. The Hamburg/ESO R-process Enhanced Star Survey (HERES). V. Detailed abundance analysis of the r-process enhanced star HE 2327-5642. *Astronomy and Astrophysics* **516**, A46 (2010).

(52) J. J. Cowan, C. Sneden, S. Burles, I. I. Ivans, T. C. Beers, J. W. Truran, J. E. Lawler, F. Primas, G. M. Fuller, B. Pfeiffer, K.-L. Kratz. The chemical composition and age of the metal-poor halo star BD +17°3248. *The Astrophysical Journal* **572**, 861-879 (2002).

(53) E. A. Den Hartog, M. T. Herd, J. E. Lawler, C. Sneden, J. J. Cowan, T. C. Beers. Improved laboratory transition probabilities for Pt I and application to the platinum abundances of BD +17°3248 and the Sun. *The Astrophysical Journal* **619**, 639-655 (2005).

(54) I. U. Roederer, C. Sneden, J. E. Lawler, J. J. Cowan. New abundance determinations of cadmium, lutetium, and osmium in the r-process enriched star BD +17 3248. *The Astrophysical Journal* **714**, L123-L127 (2010).

(55) I. U. Roederer, J. J. Cowan, M. Pignatari, T. C. Beers, E. A. Den Hartog, R. Ezzeddine, A. Frebel, T. T. Hansen, E. M. Holmbeck, M. R. Mumpower, V. M. Placco, C. M. Sakari, R.

Surman, N. Vassh. The R-Process Alliance: Abundance universality among some elements at and between the first and second r-process peaks. *The Astrophysical Journal* **936**, 84 (2022).

(56) I. I. Ivans, J. Simmerer, C. Sneden, J. E. Lawler, J. J. Cowan, R. Gallino, S. Bisterzo. Near-ultraviolet observations of HD 221170: New insights into the nature of r-process-rich stars. *The Astrophysical Journal* **645**, 613-633 (2006).

(57) C. J. Hansen, F. Primas, H. Hartman, K.-L. Kratz, S. Wanajo, B. Leibundgut, K. Farouqi, O. Hallmann, N. Christlieb, H. Nilsson. Silver and palladium help unveil the nature of a second r-process. *Astronomy and Astrophysics* **545**, A31 (2012).

(58) M. Hanke, C. J. Hansen, H.-G. Ludwig, S. Cristallo, A. McWilliam, E. K. Grebel, L. Piersanti. A high-precision abundance analysis of the nuclear benchmark star HD 20. *Astronomy and Astrophysics* **635**, A104 (2020).

(59) V. M. Placco, R. M. Santucci, Z. Yuan, M. K. Mardini, E. M. Holmbeck, X. Wang, R. Surman, T. T. Hansen, I. U. Roederer, T. C. Beers, A. Choplin, A. P. Ji, R. Ezzeddine, A. Frebel, C. M. Sakari, D. D. Whitten, J. Zepeda. The R-process Alliance: The peculiar chemical abundance pattern of RAVE J183013.5-455510. *The Astrophysical Journal* **897**, 78 (2020).

(60) S. Honda, W. Aoki, T. Kajino, H. Ando, T. C. Beers, H. Izumiura, K. Sadakane, M. Takada-Hidai. Spectroscopic studies of extremely metal-poor stars with the Subaru High Dispersion Spectrograph. II. The r-process elements, including thorium. *The Astrophysical Journal* **607**, 474-498 (2004).

(61) J. A. Johnson. Abundances of 30 elements in 23 metal-poor stars. *The Astrophysical Journal Supplement Series* **139**, 219-247 (2002).

(62) J. A. Johnson, M. Bolte. The r-process in the early Galaxy. *The Astrophysical Journal* **579**, 616-625 (2002).

(63) I. U. Roederer, J. E. Lawler, J. J. Cowan, T. C. Beers, A. Frebel, I. I. Ivans, H. Schatz, J. S. Sobeck, C. Sneden. Detection of the second r-process peak element tellurium in metal-poor stars. *The Astrophysical Journal* **747**, L8 (2012).

(64) I. U. Roederer, J. E. Lawler, J. S. Sobeck, T. C. Beers, J. J. Cowan, A. Frebel, I. I. Ivans, H. Schatz, C. Sneden, I. B. Thompson. New Hubble Space Telescope observations of heavy elements in four metal-poor stars. *The Astrophysical Journal Supplement Series* **203**, 27 (2012).

(65) I. U. Roederer, H. Schatz, J. E. Lawler, T. C. Beers, J. J. Cowan, A. Frebel, I. I. Ivans, C. Sneden, J. S. Sobeck. New detections of arsenic, selenium, and other heavy elements in two metal-poor stars. *The Astrophysical Journal* **791**, 32 (2014).

(66) I. U. Roederer, J. E. Lawler. Detection of elements at all three r-process peaks in the metal-poor star HD 160617. *The Astrophysical Journal* **750**, 76 (2012).

(67) R. C. Peterson, B. Barbuy, M. Spite. Trans-iron Ge, As, Se, and heavier elements in the dwarf metal-poor stars HD 19445, HD 84937, HD 94028, HD 140283, and HD 160617. *Astronomy and Astrophysics* **638**, A64 (2020).

(68) M. Aoki, Y. Ishimaru, W. Aoki, S. Wanajo. Diversity of abundance patterns of light neutron-capture elements in very-metal-poor stars. *The Astrophysical Journal* **837**, 8 (2017).

(69) S. Honda, W. Aoki, Y. Ishimaru, S. Wanajo. Neutron-capture elements in the very metal-poor star HD 88609: Another star with excesses of light neutron-capture elements. *The Astrophysical Journal* **666**, 1189-1197 (2007).

(70) S. Honda, W. Aoki, Y. Ishimaru, S. Wanajo, S. G. Ryan. Neutron-capture elements in the very metal poor star HD 122563. *The Astrophysical Journal* **643**, 1180-1189 (2006).

(71) J. E. Lawler, C. Sneden, J. J. Cowan, I. I. Ivans, E. A. Den Hartog. Improved laboratory transition probabilities for Ce II, application to the cerium abundances of the Sun and five r-process-rich, metal-poor stars, and rare earth lab data summary. *The Astrophysical Journal Supplement Series* **182**, 51-79 (2009).

(72) D. Radice, A. Perego, K. Hotokezaka, S. A. Fromm, S. Bernuzzi, L. F. Roberts. Binary neutron star mergers: mass ejection, electromagnetic counterparts, and nucleosynthesis. *The Astrophysical Journal* **869**, 130 (2018).'

(73) M. R. Mumpower, P. Jaffke, M. Verriere, J. Randrup. Primary fission fragment mass yields across the chart of nuclides. *Physical Review C* **101**, 054607 (2020).

(74) N. Vassh, R. Vogt, R. Surman, J. Randrup, T. M. Sprouse, M. R. Mumpower, P. Jaffke, D. Shaw, E. M. Holmbeck, Y. Zhu, G. C. McLaughlin. Using excitation-energy dependent fission yields to identify key fissioning nuclei in r-process nucleosynthesis. *Journal of Physics G Nuclear Physics* **46**, 065202 (2019).

(75) G. J. Wasserburg, M. Busso, R. Gallino. Abundances of actinides and short-lived nonactinides in the interstellar medium: Diverse supernova sources for the r-processes. *The Astrophysical Journal* **466**, L109 (1996).

(76) A. McWilliam. Barium abundances in extremely metal-poor stars. *The Astronomical Journal* **115**, 1640-1647 (1998).

(77) C. Sneden, J. J. Cowan, I. I. Ivans, G. M. Fuller, S. Burles, T. C. Beers, J. E. Lawler. Evidence of multiple r-process sites in the early Galaxy: New observations of CS 22892-052. *The Astrophysical Journal* **533**, L139-L142 (2000).

(78) W. Aoki, S. Honda, T. C. Beers, T. Kajino, H. Ando, J. E. Norris, S. G. Ryan, H. Izumiura, K. Sadakane, M. Takada-Hidai. Spectroscopic studies of very metal-poor stars with the Subaru High Dispersion Spectrograph. III. Light neutron-capture elements. *The Astrophysical Journal* **632**, 611-637 (2005).

(79) I. U. Roederer, J. J. Cowan, A. I. Karakas, K.-L. Kratz, M. Lugaro, J. Simmerer, K. Farouqi, C. Sneden. The ubiquity of the rapid neutron-capture process. *The Astrophysical Journal* **724**, 975-993 (2010).

(80) R. Cayrel, V. Hill, T. C. Beers, B. Barbuy, M. Spite, F. Spite, B. Plez, J. Andersen, P. Bonifacio, P. François, P. Molaro, B. Nordström, F. Primas. Measurement of stellar age from uranium decay. *Nature* **409**, 691-692 (2001).

(81) E. M. Holmbeck, T. C. Beers, I. U. Roederer, V. M. Placco, T. T. Hansen, C. M. Sakari, C. Sneden, C. Liu, Y. S. Lee, J. J. Cowan, A. Frebel. The R-Process Alliance: 2MASS J09544277+5246414, the most actinide-enhanced r-II star known. *The Astrophysical Journal* **859**, L24 (2018).

(82) A. P. Ji, A. Frebel. From actinides to zinc: Using the full abundance pattern of the brightest star in Reticulum II to distinguish between different r-process sites. *The Astrophysical Journal* **856**, 138 (2018).

(83) E. M. Holmbeck, A. Frebel, G. C. McLaughlin, M. R. Mumpower, T. M. Sprouse, R. Surman. Actinide-rich and actinide-poor r-process-enhanced metal-poor stars do not require separate r-process progenitors. *The Astrophysical Journal* **881**, 5 (2019).

(84) A. Perego, S. Rosswog, R. M. Cabezón, O. Korobkin, R. Käppeli, A. Arcones, M. Liebendörfer. Neutrino-driven winds from neutron star merger remnants. *Monthly Notices of the Royal Astronomical Society* **443**, 3134-3156 (2014).

(85) D. Kasen, R. Fernández, B. D. Metzger. Kilonova light curves from the disc wind outflows of compact object mergers. *Monthly Notices of the Royal Astronomical Society* **450**, 1777-1786 (2015).

(86) R. Fernández B. D. Metzger. Electromagnetic signatures of neutron star mergers in the Advanced LIGO era. *Annual Review of Nuclear and Particle Science* **66**, 23-45 (2016).

(87) T. Tsujimoto, N. Nishimura, K. Kyutoku. r-process enrichment in the Galactic halo characterized by nucleosynthesis variation in the ejecta of coalescing neutron star binaries. *The Astrophysical Journal* **889**, 119 (2020).

(88) F. L. H. Tissot, N. Dauphas, L. Grossman. Origin of uranium isotope variations in early solar nebula condensates. *Science Advances* **2**, e1501400-e1501400 (2016).

(89) M. Lugaro, A. Yagüe López, B. Soós, B. Côté, M. Pető, N. Vassh, B. Wehmeyer, M. Pignatari. Origin of plutonium-244 in the early solar system. *Universe* **8**, 343 (2022).

(90) A. Wallner, T. Faestermann, J. Feige, C. Feldstein, K. Knie, G. Korschinek, W. Kutschera, A. Ofan, M. Paul, F. Quinto, G. Rugel, P. Steier. Abundance of live ^{244}Pu in deep-sea reservoirs on Earth points to rarity of actinide nucleosynthesis. *Nature Communications* **6**, 5956 (2015).

(91) A. Wallner, M. B. Froehlich, M. A. C. Hotchkis, N. Kinoshita, M. Paul, M. Martschini, S. Pavetich, S. G. Tims, N. Kivel, D. Schumann, M. Honda, H. Matsuzaki, T. Yamagata. ^{60}Fe and

^{244}Pu deposited on Earth constrain the r-process yields of recent nearby supernovae. *Science* **372**, 742-745 (2021).

(92) A. I. Karakas, J. C. Lattanzio. The Dawes Review 2: Nucleosynthesis and stellar yields of low- and intermediate-mass single stars. *Publications of the Astronomical Society of Australia* **31**, e030 (2014).

(93) S. Wanajo, H.-T. Janka, B. Müller. Electron-capture supernovae as the origin of elements beyond iron. *The Astrophysical Journal* **726**, L15 (2011).

(94) A. Arcones, F. Montes. Production of light-element primary process nuclei in neutrino-driven winds. *The Astrophysical Journal* **731**, 5 (2011).

(95) A. D. Vlasov, B. D. Metzger, J. Lippuner, L. F. Roberts, T. A. Thompson. Neutrino-heated winds from millisecond protomagnetars as sources of the weak r-process. *Monthly Notices of the Royal Astronomical Society* **468**, 1522-1533 (2017).

(96) U. Frischknecht, R. Hirschi, M. Pignatari, A. Maeder, G. Meynet, C. Chiappini, F.-K. Thielemann, T. Rauscher, C. Georgy, S. Ekström. s-process production in rotating massive stars at solar and low metallicities. *Monthly Notices of the Royal Astronomical Society* **456**, 1803-1825 (2016).

(97) A. Choplin, R. Hirschi, G. Meynet, S. Ekström, C. Chiappini, A. Laird. Non-standard s-process in massive rotating stars. Yields of 10-150 $M_\odot$ models at $Z = 10^{-3}$. *Astronomy and Astrophysics* **618**, A133 (2018).

(98) P. Banerjee, A. Heger, Y.-Z. Qian. New s-process mechanism in rapidly rotating massive population II stars. *The Astrophysical Journal* **887**, 187 (2019).

(99) M. Lugaro, S. W. Campbell, H. Van Winckel, K. De Smedt, A. I. Karakas, F. Käppeler. Post-AGB stars in the Magellanic Clouds and neutron-capture processes in AGB stars. *Astronomy and Astrophysics* **583**, A77 (2015).

(100) M. Hampel, R. J. Stancliffe, M. Lugaro, B. S. Meyer. The intermediate neutron-capture process and carbon-enhanced metal-poor stars. *The Astrophysical Journal* **831**, 171 (2016).

(101) P. A. Denissenkov, F. Herwig, P. Woodward, R. Andrassy, M. Pignatari, S. Jones. The i-process yields of rapidly accreting white dwarfs from multicycle He-shell flash stellar evolution models with mixing parametrizations from 3D hydrodynamics simulations. *Monthly Notices of the Royal Astronomical Society* **488**, 4258-4270 (2019).

(102) C. Sneden, J. J. Cowan, R. Gallino. Neutron-capture elements in the early galaxy. *Annual Review of Astronomy and Astrophysics* **46**, 241-288 (2008).

(103) F. Käppeler, H. Beer, K. Wisshak. s-process nucleosynthesis-nuclear physics and the classical model. *Reports on Progress in Physics* **52**, 945-1013 (1989).

(104) S. Goriely. Uncertainties in the solar system r-abundance distribution. *Astronomy and Astrophysics* **342**, 881-891 (1999).

(105) D. L. Burris, C. A. Pilachowski, T. E. Armandroff, C. Sneden, J. J. Cowan, H. Roe. Neutron-capture elements in the early Galaxy: Insights from a large sample of metal-poor giants. *The Astrophysical Journal* **544**, 302-319 (2000).

(106) S. Bisterzo, C. Travaglio, R. Gallino, M. Wiescher, F. Käppeler. Galactic chemical evolution and solar s-process abundances: Dependence on the ^{13}C-pocket structure. *The Astrophysical Journal* **787**, 10 (2014).

(107) L. Mashonkina, N. Christlieb. The Hamburg/ESO R-process Enhanced Star survey (HERES). IX. Constraining pure r-process Ba/Eu abundance ratio from observations of r-II stars. *Astronomy and Astrophysics* **565**, A123 (2014).

(108) N. Prantzos, C. Abia, S. Cristallo, M. Limongi, A. Chieffi. Chemical evolution with rotating massive star yields II. A new assessment of the solar s- and r-process components. *Monthly Notices of the Royal Astronomical Society* **491**, 1832-1850 (2020).

(109) J. Simmerer, C. Sneden, J. J. Cowan, J. Collier, V. M. Woolf, J. E. Lawler. The rise of the s-process in the Galaxy. *The Astrophysical Journal* **617**, 1091-1114 (2004).

(110) I. U. Roederer, K. Hattori, M. Valluri. Kinematics of highly r-process-enhanced field stars: Evidence for an accretion origin and detection of several groups from disrupted satellites. *The Astronomical Journal* **156**, 179 (2018).

(111) D. Gudin, D. Shank, T. C. Beers, Z. Yuan, G. Limberg, I. U. Roederer, V. Placco, E. M. Holmbeck, S. Dietz, K. C. Rasmussen, T. T. Hansen, C. M. Sakari, R. Ezzeddine, A. Frebel. The R-Process Alliance: Chemodynamically tagged groups of halo r-process-enhanced stars reveal a shared chemical-evolution history. *The Astrophysical Journal* **908**, 79 (2021).

(112) Y. Hirai, T. C. Beers, M. Chiba, W. Aoki, D. Shank, T. R. Saitoh, T. Okamoto, J. Makino. Origin of Highly r-process-enhanced stars in a cosmological zoom-in simulation of a Milky Way-like galaxy. *Monthly Notices of the Royal Astronomical Society*, in press, arXiv e-prints arXiv:2206.04060 (2022).

(113) C. Sneden, J. J. Cowan, J. E. Lawler, S. Burles, T. C. Beers, G. M. Fuller. Europium isotopic abundances in very metal poor stars. *The Astrophysical Journal* **566**, L25-L28 (2002).

(114) I. U. Roederer, J. E. Lawler, C. Sneden, J. J. Cowan, J. S. Sobeck, C. A. Pilachowski. Europium, samarium, and neodymium isotopic fractions in metal-poor stars. *The Astrophysical Journal* **675**, 723-745 (2008).

(115) P. Magain. Heavy elements in halo stars: the r/s-process controversy. *Astronomy and Astrophysics* **297**, 686 (1995).

(116) D. L. Lambert, C. Allende Prieto. The isotopic mixture of barium in the metal-poor subgiant HD 140283. *Monthly Notices of the Royal Astronomical Society* **335**, 325-334 (2002).

(117) A. J. Gallagher, H.-G. Ludwig, S. G. Ryan, W. Aoki. A three-dimensional hydrodynamical line profile analysis of iron lines and barium isotopes in HD 140283. *Astronomy and Astrophysics* **579**, A94 (2015).

(118) C. Wenyuan, J. Xiaohua, S. Jianrong, Z. Gang, Z. Bo. The odd isotope fractions of barium in the strongly r-process-enhanced (r-II) stars. *The Astrophysical Journal* **854**, 131 (2018).

(119) T. T. Hansen, E. M. Holmbeck, T. C. Beers, V. M. Placco, I. U. Roederer, A. Frebel, C. M. Sakari, J. D. Simon, I. B. Thompson. The R-process Alliance: First release from the southern search for r-process-enhanced stars in the Galactic halo. *The Astrophysical Journal* **858**, 92 (2018).

(120) C. M. Sakari, V. M. Placco, E. M. Farrell, I. U. Roederer, G. Wallerstein, T. C. Beers, R. Ezzeddine, A. Frebel, T. Hansen, E. M. Holmbeck, C. Sneden, J. J. Cowan, K. A. Venn, C. E. Davis, G. Matijevič, R. F. G. Wyse, J. Bland-Hawthorn, C. Chiappini, K. C. Freeman, B. K. Gibson, E. K. Grebel, A. Helmi, G. Kordopatis, A. Kunder, J. Navarro, W. Reid, G. Seabroke, M. Steinmetz, F. Watson. The R-Process Alliance: First release from the northern search for r-process-enhanced metal-poor stars in the Galactic halo. *The Astrophysical Journal* **868**, 110 (2018).

(121) R. Ezzeddine, K. Rasmussen, A. Frebel, A. Chiti, K. Hinojisa, V. M. Placco, A. P. Ji, T. C. Beers, T. T. Hansen, I. U. Roederer, C. M. Sakari, J. Melendez. The R-Process Alliance: First Magellan/MIKE release from the southern search for r-process-enhanced stars. *The Astrophysical Journal* **898**, 150 (2020).

(122) E. M. Holmbeck, T. T. Hansen, T. C. Beers, V. M. Placco, D. D. Whitten, K. C. Rasmussen, I. U. Roederer, R. Ezzeddine, C. M. Sakari, A. Frebel, M. R. Drout, J. D. Simon, I. B. Thompson, J. Bland-Hawthorn, B. K. Gibson, E. K. Grebel, G. Kordopatis, A. Kunder, J. Meléndez, J. F. Navarro, W. A. Reid, G. Seabroke, M. Steinmetz, F. Watson, R. F. Ġ. Wyse. The R-Process Alliance: Fourth data release from the search for r-process-enhanced stars in the Galactic halo. *The Astrophysical Journal Supplement Series* **249**, 30 (2020).

(123) L. Lombardo, P. Bonifacio, P. François, C. J. Hansen, E. Caffau, M. Hanke, Á. Skúladóttir, A. Arcones, M. Eichler, M. Reichert, A. Psaltis, A. J. Koch Hansen, L. Sbordone. Chemical Evolution of R-process Elements in Stars (CERES). I. Stellar parameters and chemical abundances from Na to Zr. *Astronomy and Astrophysics* **665**, A10 (2022).

(124) A. Marconi, P. Di Marcantonio, V. D'Odorico, S. Cristiani, R. Maiolino, E. Oliva, L. Origlia, M. Riva, L. Valenziano, F. M. Zerbi, M. Abreu, V. Adibekyan, C. Allende Prieto, P. J. Amado, W. Benz, I. Boisse, X. Bonfils, F. Bouchy, L. Buchhave, D. Buscher, A. Cabral, B. L. Canto Martins, A. Chiavassa, J. Coelho, L. B. Christensen, E. Delgado-Mena, J. R. de Medeiros, I. Di Varano, P. Figueira, M. Fisher, J. P. U. Fynbo, A. C. H. Glasse, M. Haehnelt, C. Haniff, C. J. Hansen, A. Hatzes, P. Huke, A. J. Korn, I. C. Leão, J. Liske, C. Lovis, P. Maslowski, I. Matute, R. A. McCracken, C. J. A. P. Martins, M. J. P. F. G. Monteiro, S. Morris, T. Morris, H.

Nicklas, A. Niedzielski, N. J. Nunes, E. Palle, P. M. Parr-Burman, V. Parro, I. Parry, F. Pepe, N. Piskunov, D. Queloz, A. Quirrenbach, R. Rebolo Lopez, A. Reiners, D. T. Reid, N. Santos, W. Seifert, S. Sousa, H. C. Stempels, K. Strassmeier, X. Sun, S. Udry, L. Vanzi, M. Vestergaard, M. Weber, E. Zackrisson. EELT-HIRES the high-resolution spectrograph for the E-ELT. *Society of Photo-Optical Instrumentation Engineers (SPIE): Ground-based and Airborne Instrumentation for Astronomy VI* **9908**, 990823 (2016).

(125) K. France, B. Fleming, G. West, S. R. McCandliss, M. R. Bolcar, W. Harris, L. Moustakas, J. M. O'Meara, I. Pascucci, J. Rigby, D. Schiminovich, J. Tumlinson. The LUVOIR Ultraviolet Multi-Object Spectrograph (LUMOS): instrument definition and design. *Society of Photo-Optical Instrumentation Engineers (SPIE) Conference Series* **10397**, 1039713 (2017).

(126) A. Szentgyorgyi, D. Baldwin, S. Barnes, J. Bean, S. Ben-Ami, P. Brennan, J. Budynkiewicz, D. Catropa, M.-Y. Chun, C. Conroy, A. Contos, J. D. Crane, D. Durusky, H. Epps, I. Evans, J. Evans, V. Fishman, A. Frebel, T. Gauron, D. Guzman, T. Hare, B.-H. Jang, J.-G. Jang, A. Jordan, J. Kim, K.-M. Kim, Y. Kim, S. Lee, M. Lopez-Morales, C. Mendes de Oliveira, K. McCracken, S. McMuldroch, J. Miller, M. Mueller, J. S. Oh, C. Onyuksel, B.-G. Park, C. Park, S.-J. Park, C. Paxson, D. Phillips, D. Plummer, W. Podgorski, A. Rubin, A. Seifahrt, D. Stark, J. Steiner, A. Uomoto, R. Walsworth, Y.-S. Yu. The GMT-consortium large earth finder (G-CLEF): an optical echelle spectrograph for the Giant Magellan Telescope (GMT). *Society of Photo-Optical Instrumentation Engineers (SPIE): Ground-based and Airborne Instrumentation for Astronomy VII* **10702**, 107021R (2018).

(127) C. Evans, S. Cristiani, C. Opitom, G. Cescutti, V. D'Odorico, J. M. Alcalá, S. H. P. Alencar, S. Balashev, B. Barbuy, N. Bastian, U. Battino, P. Cambianica, R. Carini, B. Carter, S. Cassisi, B. Vaz Castilho, N. Christlieb, R. Cooke, S. Covino, G. Cremonese, K. Cunha, A. R. da Silva, V. D'Elia, A. De Cia, G. De Silva, M. Diaz, P. Di Marcantonio, H. Ernandes, A. Fitzsimmons, M. Franchini, B. T. Gänsicke, M. Genoni, R. E. Giribaldi, A. Grazian, C. J. Hansen, F. La Forgia, M. Lazzarin, W. Marcolino, M. Marconi, A. Migliorini, P. Noterdaeme, C. Pereira, B. Pilecki, A. Quirrenbach, S. Randich, S. Rossi, R. Smiljanic, C. Snodgrass, J. Stürmer, A. Trost, E. Vanzella, P. Ventura, D. Wright, T. Zafar. The CUBES science case. *Experimental Astronomy*, in press, arXiv e-prints arXiv:2208.01677 (2022).

Acknowledgements: We thank Ani Aprahamian, Eric Bell, Benoit Côté, Yutaka Hirai, Grant Mathews, Chris Sneden, and Michael Wiescher for sharing their thoughts on early versions of the manuscript.

Funding:

US National Science Foundation grant PHY 14-30152 (Joint Institute for Nuclear Astrophysics - Chemical Evolution of the Elements; JINA-CEE) (IUR, EMH, MRM, RS, TCB, RE, AF)

US National Science Foundation grant OISE-1927130 (The International Research Network for Nuclear Astrophysics; IReNA) (TTH)

US National Science Foundation: NOIRLab, which is managed by the Association of Universities for Research in Astronomy (AURA) (VMP)

US National Science Foundation grant AST 1716251 (AF)

US National Science Foundation grant AST 1815403 (IUR)

US National Science Foundation grant AST 1815767 (IUR)

US National Science Foundation grant AST 2205847 (IUR)

US National Science Foundation grant PHY 2020275 (RS)

US Department of Energy grant DE-FG02-95-ER40934 (RS)

US Department of Energy grant DE-SC0018232 (RS)

NASA / Space Telescope Science Institute / Hubble Fellowship grant HST-HF2-51481.001 (EMH)

NASA / Space Telescope Science Institute grant HST-GO-15657 (IUR, TCB, AF, VMP)

NASA / Space Telescope Science Institute grant HST-GO-15951 (IUR, TCB, RE, AF, TTH, CMS)

NASA / Astrophysics Data Analysis Program grant 80NSSC21K0627 (IUR)

Natural Sciences and Engineering Research Council of Canada (NV)

Swedish Research Council grant VR 2021-05556 (TTH)

Author contributions:

Conceptualization: IUR

Formal Analysis: IUR, TCB

Methodology: IUR, NV, EMH, MRM, RS

Investigation: IUR, NV

Visualization: IUR, NV, EMH, MRM, RS, JJC, TCB

Writing – original draft: IUR

Writing – review & editing: IUR, NV, EMH, MRM, RS, JJC, TCB, RE, AF, TTH, VMP, CMS

Competing interests: Authors declare that they have no competing interests.

Data and materials availability: All abundance data are sourced from the literature and available in the main text or supplementary materials. The nucleosynthesis yields are available at this Zenodo link: https://zenodo.org/record/7127232 .

Supplementary Materials

Materials and Methods

Supplementary Text

Figs. S1 to S3

Tables S1 to S6

References *(33–127)*

Science AAAS

Supplementary Materials for

Title: Observational signatures of transuranic fission fragments in stars

Authors: Ian U. Roederer[1,2]*, Nicole Vassh[3], Erika M. Holmbeck[4,5,2], Matthew R. Mumpower[6,7,2], Rebecca Surman[8,2], John J. Cowan[9], Timothy C. Beers[8,2], Rana Ezzeddine[10,2], Anna Frebel[11,2], Terese T. Hansen[12], Vinicius M. Placco[13], Charli M. Sakari[14]

Correspondence to: iur@umich.edu

This PDF file includes:

Materials and Methods
Supplementary Text
Figs. S1 to S3
Tables S1 to S6

Other Supplementary Materials for this manuscript include the following:

N/A

Materials and Methods

Stellar sample

We assemble our sample from the stellar abundance literature of the last few decades. Our sample is drawn from stars listed in the JINAbase stellar abundance database *(33)*, supplemented with our own knowledge of studies not included in JINAbase. We require that Zr, Ba, and Eu abundances are reported (i.e., detected) for each star. We require that [Ba/Eu] < −0.3 for each star, which indicates that r-process material dominates the heavy-element abundance pattern *(34)*. This cut effectively excludes stars with contributions from other processes, such as the s-process or i-process, and, as discussed in detail below, it does not interfere with one of the deviations from r-process universality (subtle variations in the [Ba/Eu] ratio). Finally, we require that an abundance of at least one of the elements Se, Pd, or Te is reported, because we are interested in studying the abundances of elements at and between the first and second r-process peaks. Our sample is complete within these requirements to the best of our knowledge.

Our sample is comprised of 42 stars spanning ≈ 2.6 dex in metallicity (−3.57 ≤ [Fe/H] ≤ −0.99) and ≈ 2.2 dex in r-process enhancement (−0.52 ≤ [Eu/Fe] ≤ +1.69). Table S1 lists the name of each star, its metallicity ([Fe/H]), its r-process enhancement ([Eu/Fe]), abundances for the elements Se through Te, and the literature references from which we have adopted the abundances. Table S2 lists the uncertainties in these abundances. Table S3 lists the abundances of the heavier r-process elements, Ba through Th, in these stars, and Table S4 lists the uncertainties in these abundances.

We homogenize the stellar abundances from the literature as follows. Stellar abundances depend directly on the atomic transition probability of each line, expressed as the log(*gf*) value, which is the log of the degeneracy of the lower level times the oscillator strength. Different stellar abundance studies may adopt different sets of log(*gf*) values for the same set of transitions, which artificially increases the statistical scatter in the set of combined abundances. Furthermore, laboratory measurements of the quantities necessary to calculate log(*gf*) values have been improved in recent years for transitions of some of the lighter r-process elements, which can improve the accuracy and precision of the stellar abundances. We therefore translate the abundances of Se through Te to a uniform log(*gf*) scale, with references given in *(46)*. These changes are always small, ≤ 0.14 dex, and typically ≤ 0.03 dex, so the impact on the literature abundances is, at most, minor. The updated log ε(X) abundances are presented in Table S1. The heavier r-process elements are generally drawn from studies that are based on modern laboratory measurements *(71)*, so no corrections are made for the abundances of these elements.

Some heavy elements (Br, Kr, Rb, In, Sb, I, Xe, Cs, Lu, Ta, W, Re, Ir, Au, Hg, Tl, Pb, Bi, and U) are omitted from our analysis because there are insufficient observations of them. Tc, Pm, Po, At, Rn, Fr, Ra, Ac, and Pa are omitted because they have no stable or long-lived isotopes. Th is discussed in a separate section below.

<u>Abundance correlations and non-correlations in our sample</u>

Figures S1 and S2 illustrate the relationships among each of the lighter r-process elements ($34 \leq Z \leq 52$) and the heavier r-process elements ($56 \leq Z \leq 78$) with the [Eu/Fe] ratios. Weighted linear least-squares fits are shown.

Figure S1 demonstrates that the correlations between the log ε(X/Zr) ratios and [Eu/Fe] are not significant ($p \geq 0.08$, whereas $p < 0.05$ would indicate significance) for X = Se, Sr, Y, Nb, Mo, Cd, Sn, and Te. The relationships are significant ($p \leq 0.002$) for X = Ru, Rh, Pd, and Ag. Figure S2 demonstrates that no significant correlations are found among the log ε(X/Ba) ratios and [Eu/Fe] for X = La, Nd, Sm, Tb, Ho, Tm, Hf, Os, and Pt. Significant ($p \leq 0.03$) correlations are found for X = Ce, Pr, Eu, Gd, Dy, Er, and Yb. Hints of similar positive correlations are suggested by the data for heavier r-process elements with limited numbers of measurements (Tb, Ho, Tm, Hf, Os, Pt; $n \leq 21$ stars). We flag these elements as being ripe for future observational studies to confirm or refute the positive trends hinted at by current data. The significant correlations for Ce and Pr ($Z = 58$ and 59) are in the opposite sense as the correlations we associate with signatures of fission fragments. In other words, their log ε(X/Ba) versus [Eu/Fe] slopes are negative, and they are consistent with zero within 2 standard deviations (σ). The cause of this behavior is unclear at present, and we also flag it as being ripe for future theoretical studies to investigate.

This behavior justifies our decision to collect these elements into five groups, as shown in Fig. 2: $34 \leq Z \leq 42$ (Panel A; no significant correlations with [Eu/Fe]), $44 \leq Z \leq 47$ (Panel B; significant positive correlations with [Eu/Fe]), $48 \leq Z \leq 52$ (Panel C; no significant correlations with

[Eu/Fe]), $56 \leq Z \leq 62$ (Panel D; no significant positive correlations with [Eu/Fe]), and $63 \leq Z \leq 78$ (Panel E; significant positive correlations, or hints thereof, with [Eu/Fe]).

We next assess the statistical significance of the correlations within each of these five element groups. For the groups shown in Panels A, C, and D of Fig. 2, the slope of the weighted linear least-squares fit is consistent with zero within 2σ for all three sets of elements. The r^2 (coefficient of determination) values for the elements shown in Panels A, C, and D indicate that only 0.2%, ≪ 0.1%, and 5%, respectively of the variations in the abundances can be associated with the correlation with [Eu/Fe], rather than random uncertainties in the abundances. Furthermore, the p-value for the Pearson correlation coefficient for each sample cannot reject the null hypothesis of zero slope at even modest significance ($p \geq 0.05$) for two of the three sets of elements; the p-value for the third set (Ba through Sm; Panel D) is 0.005 for 157 measurements, although the slope is negative and consistent with zero (-0.04 ± 0.02) within 2σ.

The groups shown in Panels B and E of Fig. 2 exhibit different behavior. Their slopes differ from zero by more than 7σ. The r^2 values for the elements shown in Panels B and E indicate that 43% and 13%, respectively, of the variations in the abundances can be associated with the correlation with [Eu/Fe]. Their p-values are also highly significant (Ru through Ag: $p \ll 0.001$ for $n = 97$ individual measurements; Eu through Pt: $p \ll 0.001$ for $n = 231$ individual measurements). These metrics collectively suggest that the relationships shown in Panels B and E of Fig. 2 are statistically significant.

Nucleosynthesis calculations: hydrodynamics, nuclear data, and fission model

The nucleosynthesis calculations presented in this work make use of the hydrodynamic simulations of binary neutron star merger dynamical ejecta from *(72)*, which considers a number of variations including the neutron star equation of state, differing treatments of neutrino transport, as well as distinct sets of progenitor masses. Here we use the simulation results reported for the case of the LS220 equation of state with a neutrino leakage scheme, since these are the conditions for which *(72)* considered a broad set of progenitor mass variations. Our adoption of these models does not necessarily imply that neutron star mergers are the only viable site of r-process nucleosynthesis. Rather, this scenario provides a reasonable set of conditions in which to explore the behavior of fissioning transuranic nuclei in an r-process environment.

We demonstrate the stabilizing effect fission deposition has on predicted abundance ratios in Fig. 3. We consider two distinct fission yield sets for neutron-rich nuclei. In the first one, we assume a fissioning species always splits in half, concentrating products near $A \sim 130$ and producing no lighter elements, such as Ag. In the second one, we adopt a proper theoretical model for the fission yields *(73)*, which makes use of the properties predicted by the finite range liquid drop model (FRLDM) for very heavy unstable species. This model produces a significant amount of fission products with $A < 130$.

When exploring variations in the fission yields, we keep all other input nuclear data the same and use the datasets described in *(16)*. These datasets include mass predictions from FRDM2012, with neutron capture and neutron-induced fission rates, and β-decay and β-delayed fission rates, determined from the LANL CoH and BeoH models, respectively. We also adopt the FRLDM fission barriers. Although significant uncertainties remain in the nuclear data for the neutron-rich nuclei populated during our nucleosynthesis calculations, and such unknowns can impact the exact abundance ratios predicted *(74)*, our result regarding fission deposition and coproduction does not depend on our choice of adopted nuclear data. Rather, the critical requirements highlighted by these calculations are (a) that the r-process reaches nuclei that fission during the times when abundances are being set, and (b) that these fission products include both lighter elements, such as Ag, and heavier elements, such as Eu, thereby linking these elements through their simultaneous production.

<u>Modeling the abundance patterns with the inclusion of fission fragments</u>

Our analysis of the abundance pattern that includes enhancements from fission fragments is constructed as follows. Our empirical template for the baseline abundance pattern is calculated using the mean abundance ratios found in the 13 stars with [Eu/Fe] $\leq +0.3$. We assume that these stars contain minimal contributions from the process responsible for producing the abundance excesses observed in Figs. 1 and 2. This assumption is justified because the star-to-star dispersion of the abundance ratios in these stars (median σ of 0.19 dex) is comparable to the typical observational uncertainties (median uncertainty of 0.22 dex). In other words, the abundance ratio dispersion in these 13 stars can be fully accounted for by the observational uncertainties.

The values of this baseline pattern, expressed as log $\varepsilon(X/Zr)_{base}$ and log $\varepsilon(X/Ba)_{base}$, are listed in Tables S5 and S6. The pattern is shown by the green line in Fig. 1. We assume that this baseline r-process pattern is present in all stars in the sample. We add enhancements of transuranic fission fragments, adopted from the models described in the previous section. We scale the level of fission fragment enhancement, F_{enh}, to the log ε(Pd/Zr) ratio for the lighter r-process elements and the log ε(Gd/Ba) ratio for the heavier r-process elements. For example, $F_{enh} = 2$ indicates 1 part baseline and 2 parts fission fragments. Mathematically, the abundance ratio for element X relative to Zr can be expressed as

$$\log\varepsilon(\mathrm{X/Zr})_{\mathrm{total}} = \log(\mathrm{F_{enh}} \times 10^{\log\varepsilon(\mathrm{X/Zr})_{\mathrm{fiss}}} + 10^{\log\varepsilon(\mathrm{X/Zr})_{\mathrm{base}}}),$$

where

$$\log\varepsilon(\mathrm{X/Zr})_{\mathrm{fiss}} = \log\varepsilon(\mathrm{X})_{\mathrm{fiss}} - \log\varepsilon(\mathrm{Pd})_{\mathrm{fiss}} + \log\varepsilon(\mathrm{Pd/Zr})_{\mathrm{base}}.$$

The values of log $\varepsilon(X)_{fiss}$ and log $\varepsilon(Pd)_{fiss}$ are adopted from the fission model with equal-mass 1.40 $M_\odot$ merging neutron stars, although the exact model selected has little influence on the result, as shown in Fig. 3. All logarithms are base 10. We use an analogous set of equations to describe the enhancements relative to the baseline abundance pattern for the heavier r-process elements, replacing Zr with Ba and Pd with Gd. The enhancements described by these equations are illustrated by the orange curves in Fig. 1.

We estimate the relative contributions from fission fragment deposition under the assumption that stars with [Eu/Fe] ≤ +0.3 contain minimal contributions from fission. According to the weighted least-squares linear fit shown in Fig. 2, the Ru through Ag abundances increase by a factor of ≈ 2 (0.30 dex) in stars with [Eu/Fe] ≈ +1.1. Thus, roughly half of the Ru through Ag in stars with [Eu/Fe] ≈ +1.1 originated as fission fragments. These elements are enhanced by an average factor of ≈ 3 (0.48 dex) in the stars with the highest r-process enhancement, revealing that fission may be responsible for up to ≈ 3/4, or ≈ 75%, of the Ru through Ag in these stars. Similarly, the Eu through Pt abundances are enhanced by an average factor of ≈ 1.7 (0.22 dex) in the stars with the highest r-process enhancement, revealing that fission may be responsible for up to ≈ 60% of the Eu and heavier lanthanide elements in these stars.

Supplementary Text

Previous investigations of deviations from r-process abundance universality

R-process universality has been generally understood to apply to heavy r-process elements, including those with $56 \leq Z \leq 72$ *(37)* and $76 \leq Z \leq 78$ *(34)*. Two important deviations from r-process universality have been identified in observations. The larger effect of the two, whose variation may span more than 1.5 dex from one metal-poor star to another, is characterized by differing abundance levels between the lighter ($34 \leq Z \leq 52$) and heavier ($Z \geq 56$) r-process elements *(49, 57, 62, 75–79)*. The abundances of the two element groups are not fully independent of one another. The abundance pattern within each of the two groups is generally consistent, once the overall abundance level has been normalized *(37, 55, 56, 68)*, with the exception of the excesses we have identified. The second effect, whose variation may span up to 0.7 dex, is characterized by differing abundance levels between the actinides (Th and U; Z = 90 and 92) and the heaviest stable r-process elements *(20, 35, 80–83)*. This effect, known as the actinide boost when the actinides are enhanced, is discussed in more detail in a separate section below. These deviations from universality may reflect a diversity of conditions within a given r-process site *(11, 83)*, multiple sites within events *(84–87)*, multiple events *(10)*, or some combination of these scenarios.

Other evidence for cosmic production of transuranic nuclei

Studies have found evidence for the cosmic production of the transuranic nuclei up to at least A = 247. The decay products of ^{244}Pu and ^{247}Cm are found in meteorites *(88, 89)*. ^{244}Pu has also been detected directly in seafloor sediments *(90, 91)*. Transuranic nuclei have not been observed in stars, and their halflives are short (≤ 80 Myr) relative to the ages of stars where they might otherwise be observable (≫ 1 Gyr).

Alternative explanations

The correlations between the log ε(Ru/Zr), log ε(Rh/Zr), log ε(Pd/Zr), and log ε(Ag/Zr) ratios and [Eu/Fe] indicates that the source of the elevated Ru, Rh, Pd, and Ag abundances is related to the source of the heavy elements, including Eu. In principle, that source could be a different nucleosynthesis process operating in a core-collapse supernova, such as the weak r-process, weak s-process, or the intermediate neutron-capture process (i-process). We can exclude any process that operates only in low- or intermediate-mass stars that pass through the asymptotic giant branch (AGB) phase of evolution, such as the main s-process *(92)*. Therefore, we compare the observed abundance behavior with predictions for the weak r-process, the weak s-process, and the i-process.

The weak r-process is associated with core-collapse supernovae, where the matter is only slightly neutron rich. The weak r-process is generally not predicted to produce substantial amounts of elements as heavy as Eu *(93–95)*. Therefore, the weak r-process is not a viable explanation for the observed abundance behavior.

The weak s-process occurs in massive, rapidly rotating stars. Models of the weak s-process in low-metallicity environments do not predict enhancement among any of the log ε(Ru/Eu), log ε(Rh/Eu), log ε(Pd/Eu), or log ε(Ag/Eu) ratios without a similar increase in the log ε(Ba/Eu) and log ε(Pb/Eu) ratios. These models predict enhancement of the log ε(Ba/Eu) and log ε(Pb/Eu) ratios by several orders of magnitude *(96–98)*. These values exceed the observed ratios, log ε(Ba/Eu) = 0.99 (σ = 0.07 dex) in the nine stars with [Eu/Fe] > +1.0 in our sample, and log ε(Pb/Eu) ≈ 0.8 ($\sigma \approx$ 0.2 dex) in other r-process-enhanced stars *(79)*. The weak s-process is also not a viable explanation for the observed abundance behavior.

The i-process has been associated with several sites, including super-AGB stars, post-AGB stars, He-core and He-shell flashes in low-mass stars, and rapidly accreting white dwarfs. Models of the i-process can produce both Pd and Eu, as well as other heavy elements *(99–101)*. In order to produce log ε(Pd/Eu) ratios similar to those observed in the nine stars with [Eu/Fe] > +1.0, log ε(Pd/Eu) = 0.71 (σ = 0.12 dex), these models predict log ε(Ba/Eu) ratios ≳ 2, which is much higher than observed in these nine stars, log ε(Ba/Eu) = 0.99 (σ = 0.07 dex). Furthermore, the i-process would need to dominate the production of Eu in the stars with the highest levels of [Eu/Fe], which is unlikely given that the abundance ratios among Eu, the lanthanide elements, and all heavier elements are consistent with the Solar System r-process ratios and models for r-process nucleosynthesis *(102)*. Therefore, the i-process is not a viable explanation for the observed abundance behavior.

We conclude that no known nucleosynthesis process, except for the deposition of transuranic fission fragments in the r-process, can explain the observed abundance behaviors.

Using [Ba/Eu] ratios as a metric to assess the relative contributions from the r- and s-process

A high percentage (>94% or so) of the Eu in the Solar System originated via r-process nucleosynthesis. In contrast, a high percentage of the Ba in the Solar System (> 85% or so) originated via s-process nucleosynthesis. This situation naturally invites the use of the [Ba/Eu] ratio (or, analogously, the log ε(Ba/Eu) ratio) as a metric to assess the relative contributions of the r- and s-process to different stars. The exact values that define "pure" r- and s-process [Ba/Eu] ratios depend somewhat on the adopted model and method, but they typically differ by > 2 dex *(103–108)*. For example, *(108)* estimates that the [Ba/Eu] ratios for "pure" r-process and "pure" s-process material are ≈ −0.9 and ≈ +1.3, respectively.

Our findings imply that the [Ba/Eu] ratio exhibits a small amount of cosmic dispersion due to the r-process itself. The eight stars in our sample with [Eu/Fe] < 0.0 exhibit [Ba/Eu] = −0.53 ±0.05 (log ε(Ba/Eu) = 1.13 ± 0.05). The nine stars with [Eu/Fe] > +1.0 exhibit [Ba/Eu] = −0.67 ±0.02 (log ε(Ba/Eu) = 0.99 ± 0.02). These differences are small but significant at about the 2.5σ level.

Fortunately, the [Ba/Eu] ratio remains an acceptable general diagnostic of the r- and s-process contributions. The differences between the low- and high-[Eu/Fe] samples are much smaller than the > 2 dex differences in the "pure" r- and s-process abundance ratios. Caution is warranted, however, when attempting to interpret slight (< 0.2 dex) enhancements in the [Ba/Eu] ratio as necessarily implying the presence of small amounts of s-process contamination to an otherwise dominant r-process pattern. Similar cautions apply to other element ratios, such as [La/Eu] *(109)* or [Ce/Eu], where small but measurable enhancements could also signal deficiencies in Eu that result from less fission fragment deposition.

A metric to assess the strength of the r-process

Reference *(16)* compared the predictions of their fission yields with a limited set of observational data, 13 r-process-enhanced stars drawn from JINABase *(33)*. That study examined the relationships between the [Ru/Eu], [Pd/Eu], and [Ag/Eu] ratios and the log ε(Eu) ratio, which they adopted as a measure of the level of r-process enrichment in a given star. That study noted no correlations between the [Ru/Eu], [Pd/Eu], or [Ag/Eu] ratios and log ε(Eu), which was consistent with the behavior expected if the Ru, Pd, and Ag originate in part as fission fragments. We repeat a similar exercise for the stars in our sample, and we find significant correlations between log ε(Eu) and each of log ε(Ru/Zr) (p = 0.03, 29 stars) and log ε(Ag/Zr) (p = 0.02, 21 stars). These correlations, while significant, are weaker than the correlations with [Eu/Fe].

We find that [Eu/Fe], rather than log ε(Eu) (or [Eu/H]), represents a more predictive metric of the strength of the r-process. It is unclear at present why this is the case. The log ε(Eu) ratios represent the amount of Eu and r-process elements present in the gas from which these stars formed. In contrast, the [Eu/Fe] ratios represent the amount of Eu and r-process elements present relative to the Fe abundance of the gas, which suggests a connection to the environment where the r-process occurred *(110–112)*. Future theoretical attempts to explore the nature and cause of this behavior will be an important step to establish the relationship between the production of transuranic elements and the site(s) of the r-process.

<u>No relation to the actinide boost phenomenon</u>

The actinide boost phenomenon is not correlated with the production of transuranic fission fragments in our data, as shown in Fig. S3, panel A. We adopt log ε(Th/Eu) as a measure of the range of actinide production relative to the lanthanide elements. We adopt log ε(Pd/Zr) as a measure of the fission fragment yields relative to the lighter r-process elements. For the 15 stars in the sample with reported Pd and Th abundances, the *p*-value for the Pearson correlation coefficient between the log ε(Th/Eu) and log ε(Pd/Zr) ratios is 0.90, indicating a non-significant correlation. Furthermore, the variation in the observed actinide abundances relative to the lanthanide abundances is much smaller than the variation observed among the fission fragments. The ranges of the log ε(Th/Eu) and log ε(Pd/Zr) ratios are 0.45 dex and 1.13 dex, respectively, which correspond to factors of 2.8 and 13.5. The fission fragment yields vary by ≈ 5 times more than the actinide variations.

As shown in Fig. S3, panel B, the relationship between the fission fragments and the actinides is also not correlated with the strength of the r-process. We adopt log ε(Pd/Th) as a measure of the amount of fission fragments relative to the actinides. We adopt [Eu/Fe] as a measure of the strength of the r-process. The log ε(Pd/Th) ratio is not correlated with the [Eu/Fe] ratio. The *p*-value for the Pearson correlation correlation coefficient between the log ε(Pd/Th) and [Eu/Fe] ratios is 0.37 for the 15 stars in our sample, indicating a non-significant correlation.

We conclude that there is no correlation between the fission fragment yields and the actinide yields in these stars.

Limitations

The baseline abundance pattern in our analysis (Fig. 1, Tables S5 and S6) is calculated empirically, rather than self-consistently with the fission component. Our analysis preserves the observed abundance ratios among Se, Sr, Y, Zr, Nb, Mo, Rh, and Pd, as shown in Fig. 1. It underpredicts the abundances for Ru and overpredicts the abundances of Ag, Cd, Sn, and Te, revealing that there is room for improvement in the models. For example, there could be a more narrow range of nuclei undergoing fission during the r-process, which could therefore narrow the range of daughter products produced. Future model explorations should aim to reproduce the full range of observed abundance behavior self-consistently, and our results signal that astronomical observations can be used to confront those models with observations.

Our conclusion that some elements originate in part via transuranic fission fragment deposition in the r-process may not be applicable to populations that are more metal-rich or contaminated by material from other processes, such as the s-process. A comparison with one particular previous study demonstrates this limitation. Ref. *(57)* examined the abundances of Sr, Y, Zr, Pd, Ag, Ba, and Eu in 71 metal-poor stars to trace the contributions from different nucleosynthesis processes to each of these elements. Taken at face value, that study reached the opposite conclusion from ours, in that it found that Pd and Ag correlated more strongly with Zr than with Eu. A closer examination, however, reveals that the two studies are probing different populations of stars. First, the stars in our sample are much more metal-poor than those in *(57)*; the median [Fe/H] in our sample is −2.62, while for the sample in *(57)* it is −1.84. Secondly, the stars in our sample are more enhanced in r-process elements than the stars in *(57)*; the median [Eu/Fe] in our sample is +0.52, while for the sample in *(57)* it is +0.43. Thirdly, the stars in our sample are less contaminated by s-process material than the stars in *(57)*. The median [Ba/Eu] in our sample is −0.55, while for the sample in *(57)* it is −0.21. The sample examined by *(57)* was assembled to include stars that would reflect a combination of nucleosynthesis processes, such as charged-particle nucleosynthesis, the weak r-process, the s-process, and the r-process. In contrast, our sample is assembled to include stars where the r-process is the dominant source of the heavy elements.

Observations of r-process elements in stars are limited to elemental abundances. Individual isotopic abundances are generally inaccessible, with only a few exceptions *(113, 114)*. Our finding that Eu and Ba are slightly decoupled when transuranic fission fragment deposition occurs suggests that measurements of the Ba isotopes in very metal-poor stars *(115–118)* may need to be reinterpreted.

Not all elements can be detected in all stars. For example, there are very few observations of Cd, Sn, Te, Hf, Os, and Pt, which limits our ability to draw reliable conclusions about their origin. This limitation is a consequence of several factors, most notably the conditions found in stellar atmospheres and the energy spacing of the electronic configurations. These factors often restrict detection of these elements to wavelengths in the ultraviolet region of the spectrum observable only from space *(46)*. Surveys to identify and characterize many more r-process-enhanced stars by the R-Process Alliance *(119–122)* and others *(123),* both today and with the next generation of optical and ultraviolet spectrographs *(124–127)*, will be essential to realize the full potential of these observational constraints.

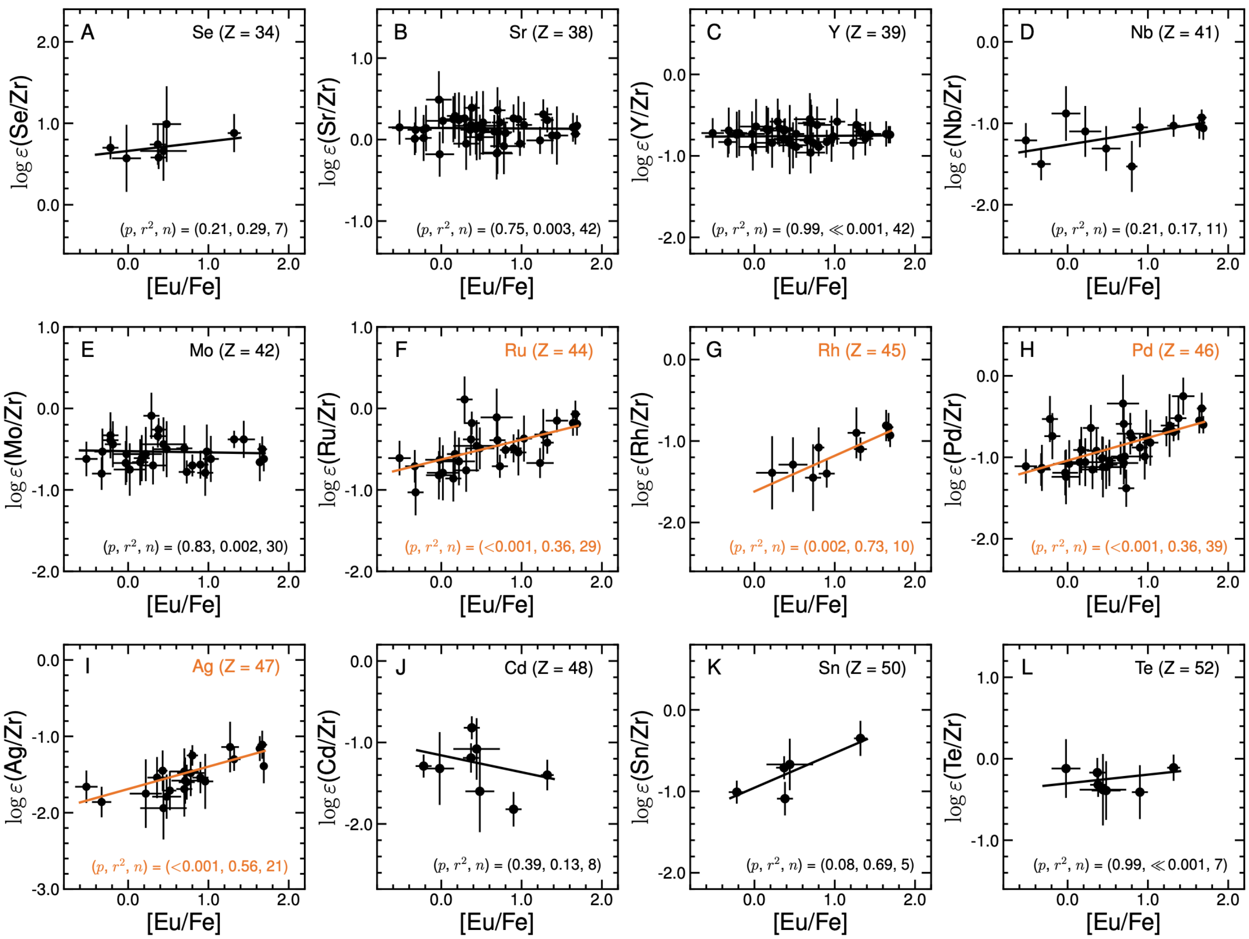

Fig. S1: Abundance ratios among the lighter elements for the 42 stars in the sample. Each point represents one star, and the errorbars represent 1σ uncertainties. Each panel illustrates the abundance ratios for a different element X (where X = Se, Sr, ..., Te) arranged by increasing atomic number, *Z*. Lines mark weighted least-squares linear fits. Non-significant trends (black lines) indicate that an element is coproduced with Zr, and significant positive correlations (orange lines) indicate that an element is coproduced with Eu. The three values printed in the lower right corner of each panel list the *p*-value for the Pearson correlation coefficient, the r^2 coefficient of determination, and the number of stars, *n*.

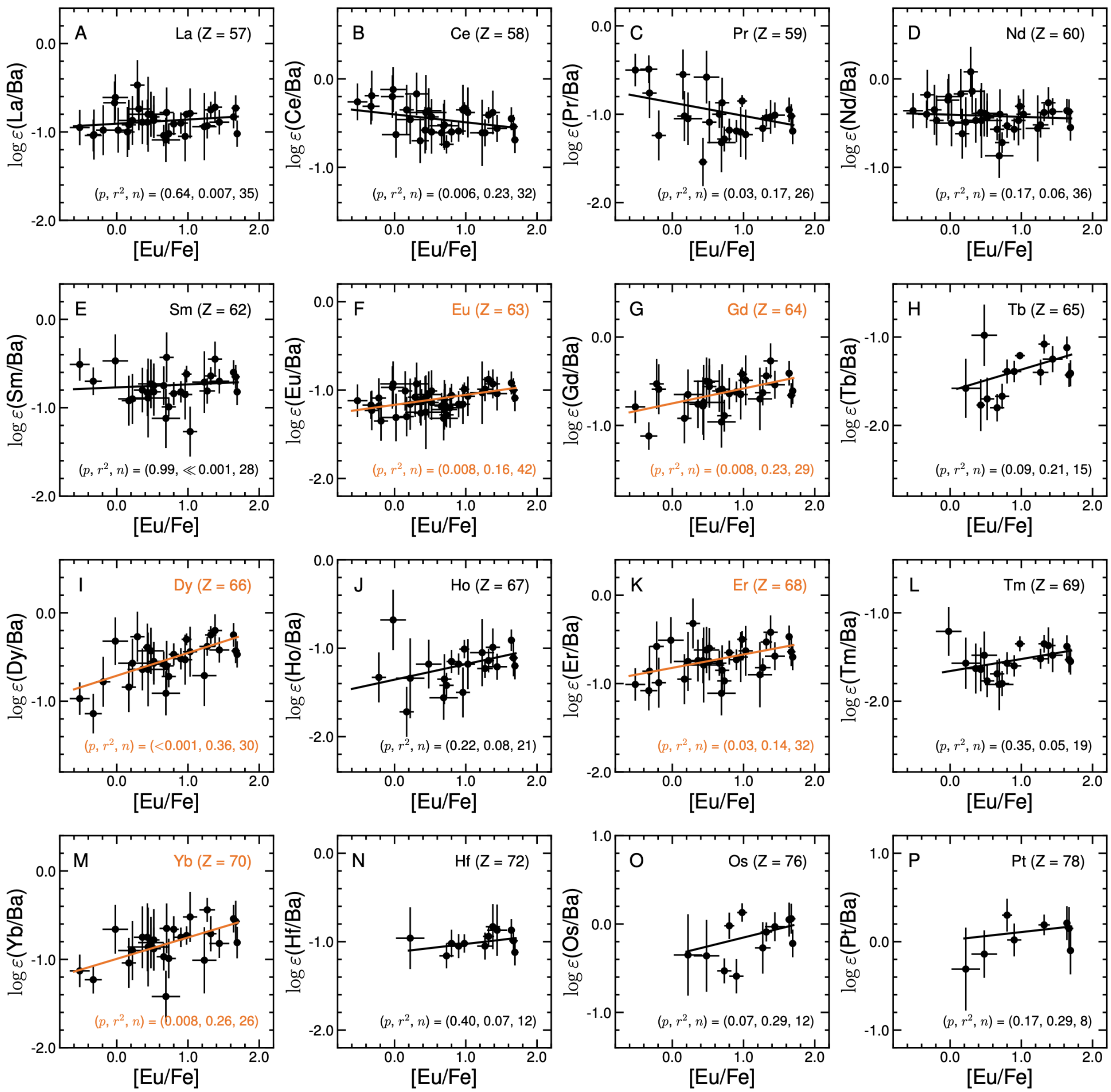

Figure S2: Abundance ratios among the heavier elements for the 42 stars in the sample. Ratios among the lanthanides (La, Ce, Pr, Nd, Sm, Eu, Gd, Tb, Dy, Ho, Er, Tm, Yb), and elements near and at the third r-process peak (Hf, Os, Pt) are shown. Each point represents one star, and the errorbars represent 1σ uncertainties. The panels are arranged by increasing atomic number, *Z*. Lines mark weighted least-squares linear fits. Non-significant trends are shown with black lines, and significant trends are shown with orange lines. The three values printed in the lower right corner of each panel list the *p*-value for the Pearson correlation coefficient, the r^2 coefficient of determination, and the number of stars, *n*.

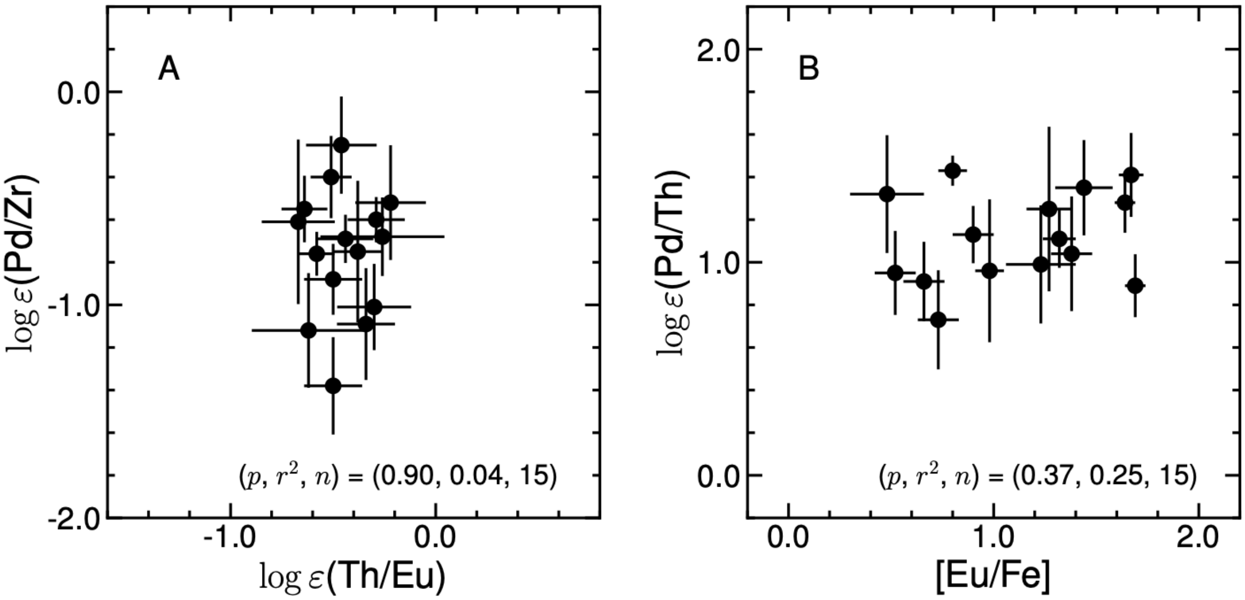

Figure S3: The relationships between the fission fragment yields (Pd) and the actinides (Th). In panel **A**, the log ε(Pd/Zr) ratio represents the relationship between the fission fragment yields and lighter r-process elements, and the log ε(Th/Eu) ratios represent the relationship between the actinides and the lanthanides. In panel **B**, the log ε(Pd/Th) ratios represent the relationship between the fission fragment yields and the actinides, and the [Eu/Fe] ratios represent the strength of the r-process. All axes span 2.4 dex. The three values printed in the lower right corner of each panel list the *p*-value for the Pearson correlation coefficient, the r^2 coefficient of determination, and the number of stars, *n*. Neither correlation is significant.

Star	[Fe/H]	[Eu/Fe]	log ε (Se)	log ε (Sr)	log ε (Y)	log ε (Zr)	log ε (Nb)	log ε (Mo)	log ε (Ru)	log ε (Rh)	log ε (Pd)	log ε (Ag)	log ε (Cd)	log ε (Sn)	log ε (Te)	Reference
CS 31082-001	-2.90	+1.69		0.68	-0.23	0.51	-0.55	-0.11	0.32	-0.42	-0.09	-0.88				*(35–38)*
CS 29497-004	-2.84	+1.67		0.72	-0.09	0.65	-0.28	0.15	0.58	-0.18	0.25	-0.46				*(39)*
CS 22892-052	-3.09	+1.64		0.41	-0.47	0.26	-0.78	-0.40	0.08	-0.55	-0.29	-0.90				*(37, 40–42)*
J1432−4125	-2.97	+1.44		0.18	-0.60	0.13		-0.25	-0.02		-0.12					*(43)*
HE 1219−0312	-2.97	+1.38		0.32	-0.52	0.27					-0.25					*(44)*
HD 222925	-1.46	+1.32	2.62	1.98	1.04	1.74	0.71	1.36	1.32	0.64	1.05	0.44	0.34	1.39	1.63	*(45, 46)*
J1538−1804	-2.09	+1.27		1.20	0.27	0.89			0.57	-0.01	0.28	-0.25				*(47)*
CS 31078-018	-2.84	+1.23		0.31	-0.52	0.32			-0.35		-0.36					*(48)*
CS 22953-003	-2.84	+1.03		0.30	-0.46	0.12		-0.50	-0.25		-0.70					*(49, 50)*
HE 2327−5642	-2.79	+0.98		-0.01	-0.72	0.04		-0.49			-0.71					*(51)*
CS 22896-154	-2.69	+0.96		0.74	-0.30	0.49		-0.30	-0.05		-0.50	-1.10				*(49, 50)*
BD +17°3248	-2.10	+0.90		1.09	0.00	0.83	-0.22	0.14	0.34	-0.57	-0.05	-0.71	-0.99		0.42	*(37, 52–55)*
HD 221170	-2.20	+0.80		0.81	-0.16	0.73	-0.80	0.03	0.22	-0.35	-0.03	-0.52				*(37, 41, 56)*
CD −45°3283	-0.99	+0.78		1.73	1.19	1.81					1.10	0.33				*(57)*
HD 20	-1.60	+0.73		1.47	0.42	1.26		0.48	0.55	-0.19	-0.12	-0.34				*(58)*
HD 120559	-1.31	+0.71		1.78	1.09	1.69					0.70	0.11				*(57)*
HD 3567	-1.33	+0.70		1.44	0.64	1.60					0.53	0.14				*(57)*
BS 17569-049	-2.88	+0.70		0.35	-0.60	-0.01		-0.50	-0.40		-0.60	-1.70				*(49, 50)*
J1830−4555	-3.57	+0.69		-1.26	-1.64	-1.09			-1.20		-1.43					*(59)*
HD 115444	-2.85	+0.66		0.05	-0.86	-0.05					-1.06					*(60)*
HD 186478	-2.60	+0.52		0.49	-0.52	0.37					-0.67	-1.34				*(61, 62)*
HD 6268	-2.63	+0.52		0.32	-0.62	0.11					-0.98					*(60)*
HD 108317	-2.37	+0.48	1.44	0.48	-0.42	0.45	-0.86	-0.05	-0.04	-0.84	-0.67	-1.34	-1.15		0.06	*(55, 63–65)*
HD 160617	-1.77	+0.44	1.71	1.22	0.25	1.05		0.61	0.59		-0.07	-0.89	-0.03	0.38	0.67	*(66, 67)*
BD +08°2548	-2.11	+0.43		0.78	-0.19	0.65					-0.36	-0.80				*(61, 62)*
HD 84937	-2.25	+0.38	1.23	1.04	-0.03	0.65		0.39	0.47				-0.17	-0.44	0.33	*(55, 67)*
HD 19445	-2.15	+0.37	1.56	1.00	0.13	0.82		0.48	0.44				-0.37	0.11	0.65	*(55, 67)*
HD 108577	-2.36	+0.36		0.35	-0.56	0.23					-0.69	-1.31				*(61, 62)*
HD 107752	-2.85	+0.31		-0.25	-0.86	-0.20		-0.90	-0.96		-1.35					*(68)*
CS 22966-057	-2.62	+0.29		0.20	-0.64	-0.06		-0.15	0.05		-0.70					*(49, 50)*
HD 126238	-1.93	+0.22		0.98	-0.10	0.74	-0.36	0.18	0.09	-0.65	-0.32	-1.01				*(64)*
HD 2796	-2.47	+0.17		0.50	-0.48	0.21		-0.40	-0.35		-0.70					*(49, 50)*
CS 29518-051	-2.69	+0.15		0.41	-0.51	0.16		-0.50	-0.70		-0.90					*(49, 50)*
HD 85773	-2.62	+0.02		0.01	-0.86	-0.22		-0.97	-1.01		-1.30					*(68)*
HD 128279	-2.46	-0.02	0.57	-0.18	-0.89	0.00	-0.88	-0.56	-0.63		-1.24		-1.32		-0.12	*(55, 63–65)*
HD 110184	-2.52	-0.03		0.46	-0.76	-0.03		-0.70	-0.85		-1.22					*(68)*
CS 22873-055	-2.99	-0.19		-0.42	-1.28	-0.56		-1.00			-1.30					*(49, 50)*
BD −18°5550	-3.06	-0.22		-1.15	-1.91	-1.17		-1.50			-1.70					*(49, 50)*
HD 140283	-2.57	-0.22	0.65	0.07	-0.77	-0.05		-0.44					-1.34	-1.06		*(67)*
CS 22873-166	-2.97	-0.32		-0.05	-0.86	-0.17		-0.70	-1.20		-1.30					*(49, 50)*
HD 88609	-3.07	-0.33		-0.19	-1.03	-0.20	-1.70	-1.00	-0.91		-1.35	-2.06				*(69)*
HD 122563	-2.77	-0.52		-0.10	-0.97	-0.25	-1.46	-0.87	-0.86		-1.36	-1.91				*(64, 69, 70)*

Table S1: Stellar abundances for lighter r-process elements, sorted by decreasing [Eu/Fe] ratios.

Star	[Fe/H] error	[Eu/Fe] error	log ε (Se) error	log ε (Sr) error	log ε (Y) error	log ε (Zr) error	log ε (Nb) error	log ε (Mo) error	log ε (Ru) error	log ε (Rh) error	log ε (Pd) error	log ε (Ag) error	log ε (Cd) error	log ε (Sn) error	log ε (Te) error
CS 31082-001	0.10	0.05		0.10	0.07	0.08	0.12	0.13	0.12	0.12	0.07	0.21			
CS 29497-004	0.12	0.06		0.11	0.08	0.07	0.07	0.14	0.15	0.16	0.18	0.17			
CS 22892-052	0.13	0.05		0.13	0.10	0.12	0.09	0.20	0.10	0.15	0.10	0.11			
J1432−4125	0.18	0.14		0.34	0.10	0.11		0.20	0.09		0.20				
HE 1219−0312	0.16	0.10		0.18	0.15	0.14					0.23				
HD 222925	0.10	0.08	0.22	0.13	0.07	0.08	0.11	0.07	0.11	0.12	0.08	0.13	0.17	0.20	0.14
J1538−1804	0.10	0.11		0.12	0.14	0.14			0.28	0.28	0.36	0.30			
CS 31078-018	0.10	0.17		0.09	0.15	0.14			0.12		0.12				
CS 22953-003	0.10	0.10		0.20	0.20	0.20		0.20	0.20		0.20				
HE 2327−5642	0.10	0.07		0.12	0.09	0.09		0.32			0.32				
CS 22896-154	0.10	0.10		0.20	0.20	0.20		0.20	0.20		0.20	0.30			
BD +17°3248	0.08	0.10		0.10	0.05	0.14	0.20	0.10	0.10	0.10	0.09	0.15	0.16		0.30
HD 221170	0.12	0.07		0.08	0.07	0.09	0.30	0.10	0.05	0.23	0.05	0.10			
CD −45°3283	0.10	0.17		0.30	0.15	0.17					0.19	0.25			
HD 20	0.04	0.10		0.26	0.09	0.09		0.11	0.11	0.40	0.21	0.21			
HD 120559	0.10	0.17		0.12	0.15	0.17					0.21	0.25			
HD 3567	0.10	0.18		0.20	0.19	0.17					0.20	0.25			
BS 17569-049	0.10	0.10		0.20	0.20	0.20		0.20	0.20		0.20	0.30			
J1830−4555	0.10	0.20		0.20	0.20	0.25			0.25		0.25				
HD 115444	0.15	0.10		0.11	0.08	0.17					0.11				
HD 186478	0.16	0.08		0.30	0.12	0.06					0.25	0.25			
HD 6268	0.11	0.10		0.33	0.06	0.20					0.17				
HD 108317	0.22	0.18	0.42	0.19	0.20	0.20	0.19	0.28	0.16	0.27	0.18	0.21	0.46		0.30
HD 160617	0.29	0.29	0.21	0.30	0.30	0.30		0.14	0.10		0.22	0.28	0.23	0.10	0.32
BD +08°2548	0.19	0.06		0.30	0.15	0.09					0.25	0.25			
HD 84937	0.10	0.10	0.10	0.10	0.10	0.10		0.10	0.10				0.10	0.18	0.11
HD 19445	0.10	0.10	0.23	0.10	0.10	0.10		0.10	0.16				0.15	0.10	0.15
HD 108577	0.13	0.12		0.30	0.13	0.10					0.25	0.25			
HD 107752	0.10	0.16		0.28	0.16	0.16		0.17	0.21		0.18				
CS 22966-057	0.10	0.10		0.20	0.20	0.20		0.20	0.20		0.20				
HD 126238	0.19	0.20		0.24	0.19	0.24	0.20	0.23	0.17	0.38	0.17	0.38			
HD 2796	0.10	0.10		0.20	0.20	0.20		0.20	0.20		0.20				
CS 29518-051	0.10	0.10		0.20	0.20	0.20		0.20	0.20		0.20				
HD 85773	0.10	0.20		0.20	0.28	0.19		0.26	0.28		0.22				
HD 128279	0.22	0.18	0.36	0.19	0.21	0.20	0.27	0.28	0.19		0.27		0.40		0.30
HD 110184	0.10	0.16		0.28	0.18	0.21		0.17	0.21		0.18				
CS 22873-055	0.10	0.10		0.20	0.20	0.20		0.20			0.20				
BD −18°5550	0.10	0.10		0.20	0.20	0.20		0.20			0.20				
HD 140283	0.10	0.10	0.10	0.10	0.10	0.10		0.10					0.10	0.10	
CS 22873-166	0.10	0.10		0.20	0.20	0.20		0.20	0.20		0.20				
HD 88609	0.20	0.12		0.12	0.10	0.16	0.12	0.12	0.12		0.12	0.12			
HD 122563	0.19	0.14		0.14	0.09	0.16	0.14	0.14	0.14		0.14	0.14			

Table S2: Uncertainties in the abundances and abundance ratios presented in Table S1. All values are expressed in dex. In cases where the original study did not present an uncertainty, or where only the statistical error was presented, we adopt a minimum total (statistical plus systematic) uncertainty of 0.10 dex. References are given in Table S1.

Star	[Fe/H]	[Eu/Fe]	log ε (Ba)	log ε (La)	log ε (Ce)	log ε (Pr)	log ε (Nd)	log ε (Sm)	log ε (Gd)	log ε (Tb)	log ε (Dy)	log ε (Ho)	log ε (Er)	log ε (Tm)	log ε (Yb)	log ε (Hf)	log ε (Os)	log ε (Pt)	log ε (Th)
CS 31082-001	-2.90	+1.69	0.40	-0.62	-0.29	-0.79	-0.15	-0.42	-0.21	-1.01	-0.07	-0.80	-0.30	-1.15	-0.41	-0.72	0.18	0.30	-0.98
CS 29497-004	-2.84	+1.67	0.35	-0.38	-0.19	-0.67	-0.02	-0.30	-0.31	-1.08	-0.08	-0.76	-0.29	-1.18	-0.22	-0.64	0.41	0.50	-1.16
CS 22892-052	-3.09	+1.64	-0.01	-0.84	-0.46	-0.96	-0.37	-0.61	-0.42	-1.13	-0.26	-0.92	-0.48	-1.39	-0.55	-0.88	0.04	0.20	-1.57
J1432−4125	-2.97	+1.44	0.03	-0.86	-0.53	-0.98	-0.34	-0.67	-0.51	-1.22	-0.39	-1.18	-0.66	-1.45	-0.79	-0.84	0.00		-1.47
HE 1219−0312	-2.97	+1.38	-0.14	-0.86	-0.52	-1.17	-0.41	-0.59	-0.41		-0.34	-1.13	-0.56	-1.51		-0.97			-1.29
HD 222925	-1.46	+1.32	1.26	0.51	0.85	0.22	0.88	0.62	0.82	0.18	1.01	0.12	0.73	-0.09	0.55	0.32	1.17	1.45	-0.06
J1538−1804	-2.09	+1.27	0.69	-0.24	0.08	-0.47	0.17	-0.12	0.06	-0.71	0.31	-0.54	-0.13	-0.83	0.25	-0.36	0.42		-0.97
CS 31078-018	-2.84	+1.23	-0.06	-1.00	-0.67		-0.62	-0.77	-0.76		-0.77	-1.11	-0.96		-1.07				-1.35
CS 22953-003	-2.84	+1.03	-0.22	-1.01	-0.60	-1.45	-0.62	-1.49	-0.71		-0.66	-1.40	-0.85		-0.74				
HE 2327−5642	-2.79	+0.98	-0.30	-1.10	-0.63	-1.15	-0.61	-0.92	-0.72	-1.51	-0.60	-1.31	-0.80	-1.65	-1.03	-1.32	-0.17		-1.67
CS 22896-154	-2.69	+0.96	-0.05	-1.10	-0.40	-1.25	-0.52	-0.90	-0.70		-0.58	-1.55	-0.75						
BD +17°3248	-2.10	+0.90	0.48	-0.42	-0.11	-0.71	-0.09	-0.34	-0.14	-0.91	-0.04	-0.70	-0.25	-1.12	-0.27	-0.57	-0.11	0.50	-1.18
HD 221170	-2.20	+0.80	0.18	-0.73	-0.42	-1.00	-0.35	-0.66	-0.46	-1.21	-0.29	-0.97	-0.47	-1.39	-0.48	-0.84	0.16	0.48	-1.46
CD −45°3283	-0.99	+0.78	1.51																
HD 20	-1.60	+0.73	0.93	-0.09	0.19	-0.35	0.21	-0.06	0.04	-0.74	0.21	-0.49	-0.04	-0.87	-0.06	-0.23	0.40		-0.85
HD 120559	-1.31	+0.71	1.09																
HD 3567	-1.33	+0.70	1.11																
BS 17569-049	-2.88	+0.70	-0.55	-1.33	-1.07	-1.42	-0.95	-0.98	-1.14		-1.15	-1.90	-1.40		-1.20				
J1830−4555	-3.57	+0.69	-1.04	-2.13	-1.57	-2.36	-1.91	-2.16	-2.00		-1.95	-2.60	-2.15	-2.85	-2.46				
HD 115444	-2.85	+0.66	-0.49	-1.53	-1.10	-1.49	-1.06	-1.24	-1.10	-2.29	-1.07		-1.26	-2.18	-1.46				-1.97
HD 186478	-2.60	+0.52	-0.55	-1.38	-1.15		-0.96	-1.30	-1.06		-1.12		-1.15		-1.33				
HD 6268	-2.63	+0.52	-0.45	-1.32	-0.88	-1.54	-0.89	-1.27	-1.01	-2.15	-1.00		-1.20	-2.22	-1.33				-1.93
HD 108317	-2.37	+0.48	-0.32	-1.12	-0.68	-0.90	-0.71	-1.05	-0.82	-1.30	-0.75	-1.50	-0.94	-1.80	-1.13		-0.68	-0.46	-1.99
HD 160617	-1.77	+0.44	0.44	-0.36	0.06		-0.03	-0.45	-0.30		-0.20		-0.35		-0.42				
BD +08°2548	-2.11	+0.43	-0.07	-0.96	-0.65	-1.61	-0.45	-0.90	-0.85	-1.84	-0.46		-0.81	-1.71	-0.82				
HD 84937	-2.25	+0.38	-0.22																
HD 19445	-2.15	+0.37	0.00																
HD 108577	-2.36	+0.36	-0.35	-1.24	-1.05		-0.82	-1.15	-1.11		-0.99		-1.09	-1.98	-1.10				
HD 107752	-2.85	+0.31	-1.09	-1.83	-1.26		-1.23												
CS 22966-057	-2.62	+0.29	-0.73	-1.20			-0.65				-1.00		-1.05						
HD 126238	-1.93	+0.22	-0.03	-0.90	-0.49	-1.08	-0.52	-0.93	-0.68	-1.61	-0.60	-1.37	-0.78	-1.60	-0.93	-0.99	-0.38	-0.34	
HD 2796	-2.47	+0.17	-0.48	-1.40	-0.83	-1.50	-1.10	-1.40	-1.40		-1.32	-2.20	-1.43		-1.52				
CS 29518-051	-2.69	+0.15	-1.01	-2.01		-1.56	-1.18												
HD 85773	-2.62	+0.02	-0.77	-1.75	-1.40		-1.27												
HD 128279	-2.46	-0.02	-1.03	-1.64	-1.15		-1.23	-1.50			-1.35	-1.71	-1.54	-2.24	-1.69				
HD 110184	-2.52	-0.03	-1.06	-1.73	-1.26		-1.30												
CS 22873-055	-2.99	-0.19	-1.31	-2.29		-2.55	-1.78		-1.90		-2.09		-2.30						
BD −18°5550	-3.06	-0.22	-1.67				-2.02		-2.20			-3.00	-2.25						
HD 140283	-2.57	-0.22	-1.09																
CS 22873-166	-2.97	-0.32	-1.54	-2.57	-1.73	-2.30	-1.72						-2.40						
HD 88609	-3.07	-0.33	-1.71	-2.75	-2.02	-2.20	-2.11	-2.41	-2.83		-2.85		-2.79		-2.94				
HD 122563	-2.77	-0.52	-1.65	-2.60	-1.91	-2.15	-2.01	-2.16	-2.44		-2.62		-2.66		-2.78				

Table S3: Stellar abundances for the heavier r-process elements, sorted by decreasing [Eu/Fe] ratios. References are given in Table S1.

Star	log ε (Ba) error	log ε (La) error	log ε (Ce) error	log ε (Pr) error	log ε (Nd) error	log ε (Sm) error	log ε (Gd) error	log ε (Tb) error	log ε (Dy) error	log ε (Ho) error	log ε (Er) error	log ε (Tm) error	log ε (Yb) error	log ε (Hf) error	log ε (Os) error	log ε (Pt) error	log ε (Th) error
CS 31082-001	0.14	0.05	0.05	0.05	0.05	0.05	0.05	0.05	0.05	0.06	0.05	0.05	0.11	0.05	0.07	0.23	0.13
CS 29497-004	0.12	0.08	0.06	0.06	0.07	0.06	0.07	0.06	0.07	0.17	0.11	0.08	0.20	0.07	0.12	0.21	0.08
CS 22892-052	0.12	0.05	0.05	0.07	0.06	0.07	0.07	0.04	0.06	0.02	0.04	0.04	0.10	0.04	0.15	0.15	0.10
J1432−4125	0.13	0.05	0.08	0.06	0.08	0.05	0.09	0.07	0.06	0.07	0.09	0.14	0.10	0.26	0.10		0.10
HE 1219−0312	0.13	0.12	0.21	0.14	0.12	0.15	0.15		0.13	0.17	0.14	0.16		0.22			0.14
HD 222925	0.06	0.07	0.07	0.08	0.08	0.08	0.08	0.09	0.08	0.12	0.08	0.08	0.19	0.10	0.09	0.10	0.11
J1538−1804	0.08	0.12	0.13	0.13	0.12	0.12	0.12	0.12	0.07	0.07	0.07	0.08	0.11	0.13	0.28		0.14
CS 31078-018	0.31	0.22	0.21		0.21	0.16	0.17		0.15	0.22	0.20		0.21				0.25
CS 22953-003	0.20	0.20	0.20	0.20	0.20	0.20	0.20		0.20	0.20	0.20		0.20				
HE 2327−5642	0.03	0.02	0.06	0.06	0.08	0.09	0.07	0.03	0.06	0.10	0.09	0.08	0.10	0.10	0.10		0.10
CS 22896-154	0.20	0.20	0.20	0.20	0.20	0.20	0.20		0.20	0.20	0.20						
BD +17°3248	0.11	0.05	0.05	0.06	0.06	0.05	0.04	0.05	0.05	0.05	0.04	0.05	0.01	0.08	0.16	0.15	0.10
HD 221170	0.11	0.06	0.04	0.07	0.08	0.07	0.14	0.08	0.06	0.07	0.08	0.06	0.10	0.11	0.10	0.15	0.05
CD −45°3283	0.15																
HD 20	0.10	0.06	0.03	0.10	0.06	0.04	0.15	0.10	0.07	0.10	0.09	0.10	0.20	0.10	0.10		0.10
HD 120559	0.17																
HD 3567	0.14																
BS 17569-049	0.20	0.20	0.20	0.20	0.20	0.20	0.20		0.20	0.20	0.20		0.20				
J1830−4555	0.15	0.20	0.20	0.30	0.20	0.30	0.25		0.20	0.20	0.20	0.25	0.25				
HD 115444	0.11	0.05	0.10	0.11	0.06	0.19	0.21	0.11	0.09		0.09	0.11	0.11				0.15
HD 186478	0.22	0.09	0.11		0.11	0.12	0.15		0.10		0.06		0.27				
HD 6268	0.17	0.05	0.11	0.17	0.08	0.21	0.17	0.17	0.14		0.13	0.07	0.17				0.10
HD 108317	0.19	0.17	0.17	0.23	0.18	0.20	0.19	0.29	0.18	0.20	0.18	0.19	0.22		0.36	0.19	0.21
HD 160617	0.30	0.30	0.30		0.30	0.33	0.30		0.29		0.30		0.33				
BD +08°2548	0.24	0.09	0.11	0.13	0.12	0.11	0.22	0.17	0.12		0.09	0.06	0.30				
HD 84937	0.10																
HD 19445	0.10																
HD 108577	0.21	0.13	0.14		0.14	0.14	0.17		0.11		0.11	0.19	0.28				
HD 107752	0.18	0.16	0.16		0.16												
CS 22966-057	0.20	0.20			0.20				0.20		0.20						
HD 126238	0.21	0.18	0.18	0.21	0.19	0.19	0.19	0.26	0.18	0.40	0.26	0.20	0.26	0.28	0.41	0.42	
HD 2796	0.20	0.20	0.20	0.20	0.20	0.20	0.20		0.20	0.20	0.20		0.20				
CS 29518-051	0.20	0.20		0.20	0.20												
HD 85773	0.18	0.18	0.19		0.19												
HD 128279	0.18	0.19	0.18		0.18	0.24			0.20	0.29	0.19	0.21	0.21				
HD 110184	0.18	0.16	0.16		0.16												
CS 22873-055	0.20	0.20		0.20	0.20		0.20		0.20		0.20						
BD −18°5550	0.20				0.20		0.20			0.20	0.20						
HD 140283	0.10																
CS 22873-166	0.20	0.20	0.20	0.20	0.20						0.20						
HD 88609	0.10	0.15	0.18	0.12	0.12	0.12	0.12		0.20		0.20		0.12				
HD 122563	0.12	0.16	0.17	0.14	0.16	0.14	0.14		0.14		0.14		0.14				

Table S4: Uncertainties in the abundances and abundance ratios presented in Table S3. All values are expressed in dex. In cases where the original study did not present an uncertainty, or where only the statistical error was presented, we adopt a minimum total (statistical plus systematic) uncertainty of 0.10 dex. References are given in Table S1.

Element X	$\log \varepsilon (X/Zr)_{base}$	standard error	n
Se	0.64	0.10	2
Sr	0.16	0.04	13
Y	-0.73	0.02	13
Zr	0.00	0.05	13
Nb	-1.17	0.11	4
Mo	-0.54	0.05	13
Ru	-0.66	0.09	10
Rh	-1.39	0.10	1
Pd	-0.99	0.06	12
Ag	-1.76	0.05	3
Cd	-1.31	0.10	2
Sn	-1.01	0.10	1
Te	-0.12	0.10	1

Table S5: The empirical baseline abundance pattern for lighter elements calculated from the abundances of the 13 stars with [Eu/Fe] ≤ +0.3. We adopt a minimum uncertainty of 0.10 dex when the number of stars, *n*, used to compute the mean is ≤ 2.

Element X	$\log \varepsilon (X/Ba)_{base}$	standard error	*n*
Ba	0.00	0.05	13
La	-0.87	0.06	11
Ce	-0.32	0.05	8
Pr	-0.80	0.11	7
Nd	-0.33	0.05	12
Sm	-0.70	0.08	5
Eu	-1.15	0.03	13
Gd	-0.77	0.08	6
Tb	-1.58	0.10	1
Dy	-0.70	0.11	7
Ho	-1.27	0.19	4
Er	-0.78	0.08	9
Tm	-1.39	0.13	2
Yb	-0.99	0.09	5
Hf	-0.96	0.10	1
Os	-0.35	0.10	1
Pt	-0.31	0.10	1

Table S6: The empirical baseline abundance pattern for heavier elements calculated from the abundances of the 13 stars with [Eu/Fe] ≤ +0.3. We adopt a minimum uncertainty of 0.10 dex when the number of stars, *n*, used to compute the mean is ≤ 2.